AD-A165 466 COMBINED DIRECT/INVERSE THREE DIMENSIONAL TRANSONIC WING DESIGN WITH VISC... (U) LOCKHEED-GEORGIA CO MARIETTA R A WEED ET AL. AUG 84 LG84-ER-0107-VOL-1 1/1

UNCLASSIFIED DTNSRDC/ASED-CR-02-84-VOL-1 F/G 20/4 NL

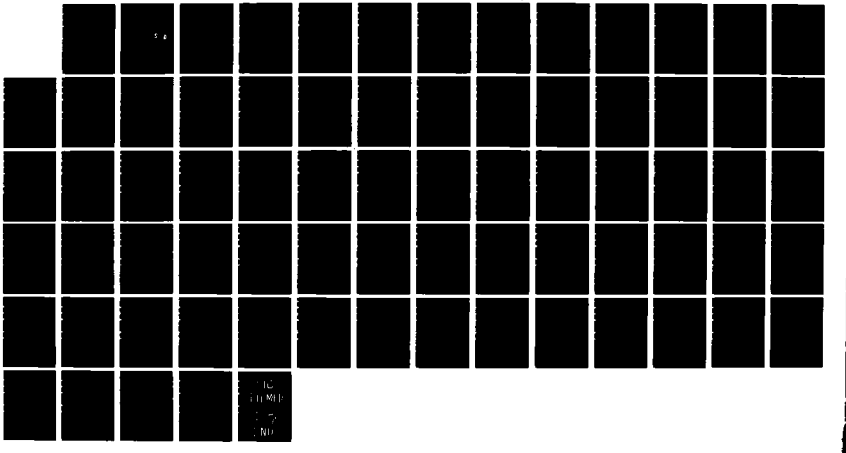

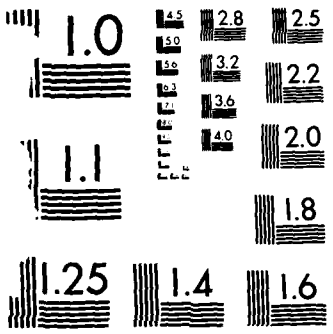

(12)

DTNSRDC-ASED-CR-02-84

COMBINED DIRECT/INVERSE THREE DIMENSIONAL TRANSONIC WING DESIGN WITH VISCOUS AND WING/BODY EFFECTS

VOLUME 1 : DESCRIPTION OF DESIGN METHOD AND RESULTS

Richard A. Weed
Lockheed-Georgia Company
Marietta, Georgia 30063

Leland A. Carlson
Texas A&M University
College Station, Texas 77843

Aug. 1984
~~February, 1986~~

Final Report for Period January 1983 to August 1984

APPROVED FOR PUBLIC RELEASE: DISTRIBUTION UNLIMITED

Prepared for

DAVID W. TAYLOR NAVAL SHIP RESEARCH AND DEVELOPMENT CENTER
Aviation and Surface Effects Department
Bethesda, Maryland 20084

UNCLASSIFIED

SECURITY CLASSIFICATION OF THIS PAGE *(When Data Entered)*

REPORT DOCUMENTATION PAGE

READ INSTRUCTIONS BEFORE COMPLETING FORM

1. REPORT NUMBER: DTNSRDC/ASED-CR-02-84	2. GOVT ACCESSION NO.
3. RECIPIENT'S CATALOG NUMBER	
4. TITLE *(and Subtitle)*: COMBINED DIRECT/INVERSE THREE DIMENSIONAL WING DESIGN WITH VISCOUS AND WING/BODY EFFECTS VOLUME 1. DESCRIPTION OF ANALYSIS/DESIGN METHOD AND RESULTS	5. TYPE OF REPORT & PERIOD COVERED: Final Report January 1983 - August 1984
	6. PERFORMING ORG. REPORT NUMBER: LG 84 ER 0107
7. AUTHOR(s): Richard A. Weed and Leland A. Carlson*	8. CONTRACT OR GRANT NUMBER(s): N00167-81-C-0078-P00004
9. PERFORMING ORGANIZATION NAME AND ADDRESS: Lockheed-Georgia Company, 86 South Cobb Drive, Marietta, GA 30063	10. PROGRAM ELEMENT, PROJECT, TASK AREA & WORK UNIT NUMBERS
11. CONTROLLING OFFICE NAME AND ADDRESS: David W. Taylor Naval Ship R&D Center, Aviation and Surface Effects Department, Bethesda, MD 20084	12. REPORT DATE: August 1984
	13. NUMBER OF PAGES: 75
14. MONITORING AGENCY NAME & ADDRESS *(if different from Controlling Office)*	15. SECURITY CLASS. *(of this report)*: UNCLASSIFIED
	15a. DECLASSIFICATION/DOWNGRADING SCHEDULE

16. DISTRIBUTION STATEMENT *(of this Report)*

APPROVED FOR PUBLIC RELEASE: DISTRIBUTION UNLIMITED

17. DISTRIBUTION STATEMENT *(of the abstract entered in Block 20, if different from Report)*

18. SUPPLEMENTARY NOTES

* Texas A&M University
College Station, TX 77843

19. KEY WORDS *(Continue on reverse side if necessary and identify by block number)*

Transonic Flow Analysis;
Inverse Wing Design;
Computational Aerodynamics;
Finite Differences.

20. ABSTRACT *(Continue on reverse side if necessary and identify by block number)*

The incorporation of wing/body and viscous flow effects into a direct/inverse transonic analysis/design method is described. Slender body theory is used to modify the transonic potential flow solver used in the analysis/design procedure to account for the effects of a fuselage on the flow characteristics of a wing in transonic flow. Viscous effects were incorporated using a modified two-dimedimensional turbulent boundary-layer program. In addition, a method for enforcing a desired trailing edge thickness during the inverse design process

(Continued on reverse side)

DD FORM 1 JAN 73 1473 EDITION OF 1 NOV 65 IS OBSOLETE

UNCLASSIFIED

SECURITY CLASSIFICATION OF THIS PAGE *(When Data Entered)*

(Block 20 Continued)

is presented. Results are presented that confirm the accuracy of the method for both analysis and design modes.

TABLE OF CONTENTS

LIST OF FIGURES

LIST OF FIGURES

NOMENCLATURE

M	- Freestream Mach number
Re	- Reynolds number
Cp	- Pressure coefficient
X,Y,Z	- Cartesian coordinates
X/C	- Airfoil X coordinate normalized by the local chord
Z/C	- Airfoil Z coordinate normalized by the local chord
ETA,η	- Normalized distance along the semi-span (2Y/B)
B	- Span length
r	- Fuselage cross-sectional radius
l	- Fuselage length
S	- Fuselage cross-sectional area
X_F, Y_F, Z_F	- Fuselage coordinates
AR	- Aspect ratio
Λ_{le}	- Leading edge sweep angle
λ	- Taper ratio
θ_r	- Root section twist angle
θt	- Tip section twist angle
α,AOA	- Angle of attack

ABSTRACT

The incorporation of wing/body and viscous flow effects into a direct/inverse transonic analysis/design method is described. Slender body theory is used to modify the transonic potential flow solver used in the analysis/design procedure to account for the effects of a fuselage on the flow characteristics of a wing in transonic flow. Viscous effects were incorporated using a modified two-dimensional turbulent boundary layer program. In addition, a method for enforcing a desired trailing edge thickness during the inverse design process is presented. Results are presented that confirm the accuracy of the method for both analysis and design modes.

ADMINISTRATIVE INFORMATION

The work presented was a joint effort by Lockheed-Georgia Company and Texas A&M University supported by the Naval Air Systems Command under the cognizance of D. G. Kirkpatrick ((NAVAIR-310D AIRTASK WR02302), Navy Contract N00167-81-C-0078-P00004. The authors acknowledge the support of Dr. Tsze C. Tai, contract technical monitor at the David Taylor Naval Ship Research and Development Center during all phases of this research.

INTRODUCTION

The results presented in this report document the work performed during the second phase of a two phase research program to develop a combined direct/inverse transonic wing design method. During the first phase of this contract, the wing design method was developed and verified for simple wings with no twist.[1] The principal tasks performed during the second phase of the contract were to extend the design method to include both wing/body and viscous effects and to incorporate an efficient method for enforcing a desired trailing edge thickness constraint during the design process. In addition, an effort was made to verify the combined analysis/design computer code developed during the course of the research for arbitrary wing planforms that possess both twist and taper.

REVIEW OF COMBINED DIRECT/INVERSE DESIGN PROCEDURE

The combined direct/inverse design procedure developed in the first phase of this research program is an extension of the direct/inverse design procedure developed by Carlson[2] for two-dimensional transonic airfoil design to three-dimensional transonic wing design. As in other inverse design procedures, the inverse design method developed in this research program computes wing sectional airfoil shapes for a prescribed pressure distribution. In the direct/inverse design procedure, a certain percentage of the leading edge region of the airfoil (usually the first 10 per cent of chord) is specified. The remaining portion of the airfoil is computed from the prescribed pressure distribution. The direct/inverse design procedure relies on a fast and accurate transonic potential flow solver to compute the flow field in both the fixed leading edge region and the inverse region. In the inverse region, the normal wing surface boundary condition used by the solver is replaced by a specified value of potential extracted from the design pressure distribution. The potential flow solver is run until the solution reaches a desired level of convergence. The normal surface boundary condition and the velocities resulting from the specified potential can then be used to compute sectional airfoil slopes which can be integrated to give the airfoil shape. A complete description of the development of the inverse design procedure and the transonic potential flow solver used in the procedure is given in Reference 1.

TRAILING EDGE CLOSURE PROCEDURE

The wing shapes generated by the combined direct/inverse wing design procedure used in the present research depend on the nose shape specified in the direct-mode region and the desired pressure distribution in the inverse-mode region. Therefore, a target pressure distribution that is inconsistent with a given nose shape will produce physically unrealistic airfoils with excessively open or "fishtail" trailing edges. Carlson[2] demonstrated that the trailing edge thickness of an airfoil generated by the direct/inverse method could be controlled by varying the airfoil nose shape by trial and

error until a desired trailing edge thickness was attained. However, this trial-and-error approach is impractical for three dimensional design. Therefore, several different methods for modifying the nose shape to enforce trailing edge closure as the inverse solution progressed were investigated.

The method that has proved to be the most successful in enforcing trailing edge closure was used by Malone[3] in a subsonic wing design code. In this method, a linear thickness function is added or subtracted to the base wing geometry during the course of the solution. This function is formed by computing the difference between the current computed trailing edge thickness and a desired trailing edge thickness. A new airfoil shape is then computed with the following equation,

$$Z/C_{new} = Z/C_{old} + (Z/C_{te,desired} - Z/C_{te,computed})\ (X/C) \qquad (1)$$

This procedure has been implemented into the inverse design method in the following manner:

1. The inverse method is allowed to run a fixed number of iterations (usually 50 iterations) before the first modification to the wing shape is performed.
2. A new airfoil shape is then computed at each design station.
3. The difference between the desired and computed trailing edge thickness is calculated and used in Eq. (1) to update the airfoil shape.
4. The new airfoil shapes are used to compute the surface boundary conditions for the direction-mode region of the inverse solution.
5. Steps 2 through 4 are repeated at a fixed frequency (every 10 or 20 iterations) until the solution has converged to a desired level.

A series of tests were conducted using two different wings to verify the effectiveness of the trailing edge closure procedure. The first tests were conducted using the ONERA M6 wing used in Ref. 1 to verify the inverse design method. In these tests, the upper surface pressure distribution

generated by an analysis of the ONERA M6 wing at a Mach number of 0.83 and angle of attack of 3.06 degrees was modified at five spanwise stations near the center of the wing. This modified pressure distribution was then used as the target pressure distribution for the inverse code. The inverse boundary conditions were applied at all 20 spanwise stations used in the tests. The base and target pressure distributions for these tests are shown in Figure 1. The inverse code was run with and without the trailing edge closure procedure in effect. The airfoil shapes generated without the trailing edge procedure are shown in Figure 2. The shapes generated with the trailing edge procedure are shown in Figure 3. For these tests, the desired upper surface trailing edge ordinate was set to 0.001 at every spanwise station. It is evident that without the trailing edge closure procedure the resulting airfoil shapes are physically unrealistic or impractical for a real wing. A comparison of the original ONERA M6 analysis pressures, the target pressures and the pressures obtained from analysis of the redesigned wing are given at all 20 span stations in Figure 4. The pressures for the redesigned wing are in excellent agreement in the inverse region of the wing (in this case the aft 80 per cent of the wing). As would be expected, the pressures in the direct-mode region have changed since the relofting required to enforce trailing edge closure alters the leading edge of the wing. These results indicate that the trailing edge closure procedure is effective in enforcing a desired trailing edge thickness and the resulting wing is consistent with the specified target pressures.

A second series of tests were conducted to verify the method for wings with twist using the C5A wing planform. As in the ONERA M6 tests, the pressure distributions generated by an analysis of the C5A wing at a Mach number of 0.775 and an angle of attack of 2.0 degrees were modified to provide target pressure distributions for the inverse method. The base wing pressure distribution and the modified target pressure distribution are compared in Figure 5. As shown in Figure 5, the base wing pressure distribution was modified at 15 of the 20 spanwise design stations. The target pressure distributions for this case were generated by modifying the base pressure distributions to weaken the shock strength at each design

station. The inverse design was performed at the same Mach number and angle of attack used to generate the base wing pressure distribution. The airfoil shapes resulting from the given target pressure distribution are compared with the base C5A wing in Figure 6. The pressures for the redesigned wing are compared with the base pressures and the target pressures in Figure 7.

IMPLEMENTATION OF WING-BODY EFFECTS

The effect of a fuselage on the flow characteristics of a base wing was implemented into the analysis/design code using slender body theory.[4] The perturbation to the velocity potential due to the fuselage is taken that consist of an axial flow and a cross-flow component. The fuselage is replaced by a line of doublets. By assuming the fuselage to be a slender body, the doublet strength for the axial flow component can be taken to be proportional to the derivative of the cross-sectional area distribution of the fuselage in the axial direction. The doublet strength for the cross-flow component is proportional to the cross-sectional area distribution of the fuselage. A spanwise velocity component at the wing root can be computed using the following equation.

$$V_F = \cos\alpha \frac{Y_F}{4\pi} \beta^2 \int_0^1 \frac{S'(\xi)d\xi}{((X_F-\xi)^2 + \beta^2 r_F^2)^{3/2}} - \frac{3Y_F Z_F}{2\pi} \int_0^1 \frac{S(\xi)d\xi}{((X_F-\xi)^2+r_F^2)^{5/2}} \qquad (2)$$

where

β = $1 - M_\infty^2$
r^2 = $Y_F^2 + Z_F^2$
$S(\xi)$ = cross-sectional area of fuselage
$S'(\xi)$ = $d S/d\xi$
l = total length of fuselage

The orientation of the fuselage coordinate system and the wing coordinate system is shown in Figure 8.

As shown by Schlichting and Truckenbrodt[5], the effect of the fuselage on the wetted portion of the wing for the case of a mid-fuselage mounted wing is an increase in span loading due to an increase in upwash on the wing. A typical mid-wing configuration (the RAE wing given in Ref. 6) was used to test the implementation of the wing/fuselage effects. The pressure distribution for four different span locations are compared with the wing alone pressure distribution in Figure 9. The span loading distributions for the wing/body and wing alone case are given in Figure 10. These results indicate that the expected effect of the body on the vetted wing is produced by the current procedure.

VISCOUS INTERACTION CORRECTION

At transonic speeds, experimental evidence indicates that viscous interaction effects can significantly affect both the pressure distribution on the wing and the resultant aerodynamic force coefficients. For example, a wing using aft-cambered airfoil sections which is designed inviscidly for transonic conditions may actually in practice develop 25 to 50 percent less lift than predicted by the inviscid procedure. This loss in lift is due not only to the existence of a boundary layer displacement surface on the wing, which changes the effective shape of the wing, but also to such factors as wake curvature and vertical pressure gradients in the trailing edge region. To prevent such discrepancies, the effects of at least weak viscous interaction should be included in both the analysis and design portions of any transonic analysis/design numerical method. It should be noted that in this report the term weak viscous interaction implies that there is no massive boundary layer separation anywhere on the wing. Nevertheless, for many wings at transonic conditions, the effects of viscous interaction on wing performance can still be quite large.

In the present program, the basic approach is to assume that the three-dimensional inviscid flowfield follows a displacement surface with ordinates and slopes different from those of the actual wing. While it is true that the inviscid flowfield does not exactly follow the displacement

surface in the vicinity of the trailing edge of the wing and that it is influenced by the effects of wake curvature, such effects are assumed in the present approach to be either secondary or capable of being handled empirically. At those wing stations where the airfoil sections are designed using the inverse procedure, the approach is to treat the airfoil section determined by the inverse technique as the displacement surface for that section and to subtract from it the displacement thickness determined by an appropriate boundary layer computation. Usually, this subtraction is performed after the inverse design procedure has converged, and the resultant ordinates are considered to be the actual airfoil ordinates for rthe designed stations.

For those portions of the wing which are not being designed and for which the actual section airfoil ordinates are assumed known, viscous correction is included as if those portions were being analyzed (i.e., wing ordinates are given as well as the flowfield and pressure distribution to be determined). At these analysis stations, the approach is to calculate a boundary layer displacement surface (i.e., airfoil ordinate plus displacement thickness) and then to compute the inviscid flowfield using the resultant displacement surface. Since viscous correction can significantly affect the pressure distribution and flowfield, the computation of the boundary layer and the displacement surface must be performed at regular intervals throughout the iterative computation of the inviscid flowfield. In this manner, the convergence rate at analysis stations is enhanced, and the final solution at those stations should reflect the effects of weak viscous interaction in a coupled manner.

Obviously, the key to properly including viscous correction is to utilize a boundary layer computation method which accurately yields displacement thicknesses and hence the resultant displacement surface. Such a boundary layer scheme must be reliable, reasonably accurate, and computationally very efficient. The latter requirement is very important since the boundary layer in the analysis regions must be updated many times throughout a complete calculation. In addition, the viscous method must be

computationally robust in the sense that it must not fail (i.e., cause the program to terminate computations) when phenomena such as premature separation occur near the trailing edge of the wing or in the vicinity of shock waves. Frequently, such effects do occur during the initial stages of computation, particularly near shock waves and in the cove region on aft-cambered airfoils, even though they do not exist in the final converged solution.

In selecting an appropriate boundary layer calculation method, the code developer is faced with many possibilities. Obviously, the most complicated and perhaps most accurate choice would be a fully three-dimensional turbulent compressible technique. However, such methods are computationally intensive (hence, expensive and time consuming), and in most cases, they have not been extensively validated against experimental data. Also, they are very difficult to couple to the inviscid transonic computational scheme. Thus, three dimensional methods are not really suitable for inclusion in an analysis/design technique developed primarily for use in preliminary design.

At the other extreme, the simplest approach would be to use a simple proven two-dimensional compressible turbulent boundary layer method and to apply it using straight-forward two-dimensional strip theory at the various wing stations. While this approach has been used by many previous investigators and certainly gives an indication of viscous interaction trends, it usually underpredicts the magnitudes of the displacement thicknesses. In a design case, such an approach could lead to theoretical airfoil section shapes which do not meet the performance expectations indicated by the theory. Nevertheless, the idea of using a two-dimensional technique is attractive from the standpoint of computational efficiency and ease of incorporation into the inviscid computational scheme.

Approximately a decade ago, Nash and Tseng[7] extensively investigated the Orpossibility of using two-dimensional techniques to compute the turbulent boundary layer on an infinite yawed wing. By comparing with three-dimensional results, they determined that a two-dimensional calculation

performed normal to the wing leading edge yielded good results for the variation and magnitude of the displacement thickness. On the other hand, they discovered that a calculation performed in the streamwise direction seriously underpredicted the magnitude of the displacement thickness but did correctly predict the magnitude of the resultant shear stress. They also rdetermined that the primary reason for the displacement thickness error was that the freestream two-dimensional calculation sensed pres sure gradients considerably less than those effectively influencing the actual boundary layer growth. Based on these conclusions, Nash and Tseng modified the governing boundary layer equations and devised a technique which used a two-dimensional calculation normal to the wing leading edge and which yielded results in excellent agreement with three-dimensional computations. They referred to this method as a "modified chord technique."

As a consequence of the results of Nash and Tseng, it was decided to use in the present analysis/design wing program a two-dimensional boundary layer scheme suitably modified to account for at least the first order effects of three dimensionality on viscous interaction. Thus, in the present method it is inherently assumed that at least locally the boundary layer growth and behavior on the wing is like that on an infinite swept wing. This approach has the advantage of being able to utilize a well-proven robust two-dimensional turbulent boundary layer scheme which is computationally efficient, and it should be adequate for wings of moderate and medium sweep angle.

Unfortunately, the modified chord technique is not directly suitable for incorporation into the present program in that it still solves a system of partial differential equations and therefore is time-consuming. Also, it is only strictly applicable to incompressible flow. In addition, its usage would require extensive interpolation and extrapolation in order to determine the pressures and coordinates along lines normal to the leading edge (or the average sweep line). Such calculations quite possibly would introduce inaccuracies which might obliterate its attempt at improvement. On the other hand, Nash and Tseng[7] showed that the streamwise computation,

which meshes well with the present inviscid coordinate system, was incorrect in its calculation of displacement thickness only because it utilized the wrong pressure gradients.

Consequently, it was decided to use a two-dimensional turbulent boundary layer calculation method in the streamwise direction at the various wing sections modified so as to use the effective pressure gradients. Based upon simple wing sweep theory and the results of Nash and Tseng, such a correction simply involves increasing the streamwise pressure gradients by a factor of one over the cosine squared of the average sweep angle. While this approach is highly approximate, it should yield good values for the displacement thicknesses and be a significant improvement over results obtained using simple strip theory. In addition, it should be adequate for preliminary analysis and design, and its inaccuracies should be compatible with those associated with assuming point transition to turbulent flow.

After extensive investigation of various two-dimensional turbulent boundary layer methods, the Nash-Macdonald method[8] together with a modified pressure gradient input and certain smoothing operations, was selected for incorporation into the present program. This method was primarily selected because it yields excellent predictions of displacement thicknesses in two-dimensional flows and because of its computational robustness and efficiency. In this method, the displacement thickness at the trailing edge of a wing airfoil station is always determined by linear extrapolation from the previous two upstream grid point values. As a result, the basic approach used here is similar to that used in the two-dimensional transonic inverse analysis/design program TRANDES.[9]

In this method, the displacement thicknesses are obtained by solving the momentum integral equation for the momentum thickness using the formulas of Nash and Macdonald for skin friction and the shape factor. This computation is performed on the same grid spacing as the corresponding inviscid solution. The result ant displacement thicknesses are then smoothed and extrapolated to obtain the thickness at the trailing edge of each section.

Normally, this smoothing is per formed twice on the medium grid and four times on the fine grid each time the boundary layer is computed.

This smoothing and extrapolation process appears to have two consequences. First, it reduces the rapid variations in the solution which sometimes occur in regions with high pressure gradients. Second, based on comparisons with two-dimensional experiments, the Nash-Macdonald method with smoothing and extrapolation seems to yield a trailing edge behavior that is correct with respect to the effect of the boundary layer on pressure distribution and lift. Admittedly, this behavior is fortuitous; however, it should serve as a reasonable engineering and preliminary design model.

In actual application, it is inefficient and inappropriate to include viscous correction on coarse grids due to the inherent pressure and flowfield inaccuracies associated with such grids. Consequently, the viscous correction procedure is not normally initiated until the fiftieth cycle of the medium grid. At that point the displacement thicknesses are computed at each appropriate wing station (i.e., analysis stations or surfaces) at the same chordwise coordinates as the inviscid grid, and the displacement surface ordinates are updated using under-relaxation. The slopes are then determined from cubic splines through the new ordinates, which are normally updated by the new boundary layer calculations every ten iteration cycles thereafter. The actual point at which the boundary layer calculations are initiated and frequency of updating are, however, controllable by the user via input data. A flow chart of the viscous design procedure with relofting is given in Figure 11.

It should be noted that while this approach does properly account for the effects of weak viscous interaction at both analysis and design wing stations, no attempt has been made to account for massive separation at the wing trailing edge or at the shock wave. The reason for this approach is that the present method is primarily a design tool, and it is unlikely that an aerodynamicist would deliberately attempt to design a transonic wing with extensive viscous separation. In addition, while considerable progress has

been made in developing coupled inviscid and boundary layer techniques to handle massively separated flows in two-dimensions, these techniques are not readily or reliably extendable to three dimensional cases.

VERIFICATION OF THE ANALYSIS METHOD FOR ARBITRARY WINGS

In the first phase of the contract, only simple wings with no twist were used to verify the analysis/design code in the analysis mode. During the course of the current research, a series of tests were made to verify the analysis code for wings with arbitrary planforms and twist distributions. The planform properties of the wings used in both the analyses and design tests are given in Appendix A. The results from these tests were correlated with both experimental data and results from other analysis codes.

SUGGESTED WING DESIGN PROCEDURE

The inverse design procedure developed in this research is appropriate for use as a preliminary design tool. Although the ability to design both the upper and lower surfaces simultaneously was included in the design code, it is suggested that the two surfaces should be designed separately. It is also suggested that the wing should be designed initially without viscous effects to get a first guess for the nose shape that will satisfy the inviscid trailing edge closure constraints. The results of the trailing edge closure procedure presented previously in this report demonstrate the problems associated with specifying inverse design pressures for an entire wing surface. The resulting airfoil shapes can vary drastically between design stations. Since most wings are manufactured by lofting the airfoil shapes between specified control stations along the span, it is suggested that a similar procedure be followed when performing a wing design with the present design procedure. The wing should be designed by performing the inverse design procedure at control stations along the wing starting at the wing root and proceeding outward along the span to the wing tip. The wing shapes for the remaining stations on the wing can be generated by lofting between the control stations.

RESULTS AND DISCUSSION

The results from the tests performed to verify the viscous flow modifications for analysis and design and the results from the analysis mode verification tests are presented in the following sections.

ANALYSIS VERIFICATION

The results for the three wing planforms described in this section were generated using a sequence of three grids. The finest grid used in the initial tests had 90 streamwise points of which 50 were on the wing surface at each span station, 30 spanwise points of which 20 were on the wing surface, and 30 points in the normal (Z) direction. A normal analysis run encompassed 200 iterations on the coarsest grid, 300 iterations on the intermediate grid, and 200 iterations on the fine grid.

WING C

The analysis results for WING C are compared with experimental data[10] in Figure 12. Corrections to both experimental angle of attack and the Mach number were made in order to match the inviscid analysis and the experimental lift coefficients. It was found by numerical experiment that the best correlation was obtained by decreasing the Mach number from 0.85 to 0.83 and the angle of attack from 5.9 to 5.0. These corrections are the same as those used by Holst et al.[11] to correlate results from the TWING program with experimental data.

WING A

WING A is a medium aspect ratio wing that is typical of the type of wing found on modern transport aircraft. The inviscid wing pressure distributions are compared with experimental data[10] in Figure 13. As in the case of WING C, corrections were made to both the Mach number and angle of

attack in order to match the experimental lift coefficients. For WING A the best correlation was obtained when the Mach number was decreased from 0.82 to 0.80 and the angle of attack was reduced from 2.5 to 1.2. Even with the large correction in angle of attack, the error induced at the outboard stations by the viscous effects is evident.

F14A FIGHTER WING

The F-14A fighter wing planform given in Reference 12 was analyzed at a Mach number of 0.80 and an angle of attack of 1.4 degrees. The leading edge sweep for this case was fixed at 20 degrees. The pressure coefficients for this configuration are compared with experimental data from Reference 12. The experimental data used in this correlation is flight test data. Therefore, the effects of the F14 body and wing glove are evident at the inboard stations. These effects along with the effects of viscous flow account for the discrepancies in the data at the two inboard stations shown in Figure 14. The correlation improves for the two outboard stations. However, the inviscid analysis still overpredicts the shock strength and location.

VISCOUS ANALYSIS AND DESIGN

The ONERA M6 wing at a Mach number of 0.84 and an angle-of-attack of 3.06 degrees was the primary test case used to verify the viscous analysis and design options in the present method. Normally, viscous calculations were initiated after fifty iterations on the intermediate grid and subsequently performed every ten iterations thereafter until the desired level of convergence was achieved. After each set of viscous calculations, the generated displacement thicknesses were used to modify the original airfoil sections at the analysis stations and the direct portions of the design stations so as to generate appropriate fluid airfoils and surface boundary conditions for the subsequent inviscid calculations. Of course, at the design stations the design pressure coefficients determined the appropriate boundary conditions. Normally, for the inverse verification tests only one design station was used.

Viscous Analysis Verification

The viscous and inviscid pressure distributions for the ONERA M6 wing are compared with experimental data in Figure 15. Here, it should be noted that the viscous calculations were obtained for a root chord Reynolds number of 25 million while the experimental data were obtained for an average wing Reynolds number of 11.75 million. Thus, some differences between the two results should exist. As can be seen on Figure 15, the viscous effects on the lower surface of the ONERA wing are quite small and on the upper surface seem only to affect the location of the shock wave. Here both the invisid and viscous calculations were performed using the experimental Mach number and angle-of-attack. Since accurate values of the tunnel corrections and experimental lift coefficient are unknown for these tests, interpretation of these results is difficult. Nevertheless, the viscous results have the correct trend in that they yield a lower lift coefficient than the inviscid calculations and the shock waves tend to be further forward. Thus, it can be concluded that the viscous analysis results are correct in trend and magnitude.

Typical displacement surface results that correspond to the conditions shown on Figure 15 are shown on Figure 16. Here it can be seen that the lower surface displacement thicknesses are smooth and quite small, which explains the lack of significant viscous effects on the lower surface. On the upper surface, however, the magnitude of the displacement thicknesses is considerably larger and the presence of the shock wave is vividly shown by the presence of a bump in the displacement surface curves. This bump is primarily due to shock boundary layer interaction; and its main effect is to move the shock wave slightly forward, as shown on the pressure distributions in Figure 15.

A second test was conducted using WING A in order to verify the viscous analysis method for wings with twist. WING A, because it was aft-cambered and supercritical. was expected to have significant viscous effects; and

this fact is verified on Figure 17 which compares the viscous and inviscid pressure distributions with the WING A experimental data. Here, the inviscid calculation had to be conducted at a significantly lower angle-of-attack than the experimental value in order to match the experimentally determined lift coefficient. Nevertheless, the lower surface pressures did not agree with the experiment in the vicinity of the aft-cambered region. On the other hand, the viscous angle-of-attack required was considerably closer to the tunnel value; and the viscous lower surface pressures are in much better agreement with the experimentally measured values. In addition, the viscous results demonstrate the expected forward movement of the shock wave locations. At some span locations, it appears that the present method overpredicts the amount of shock boundary layer interaction. It is believed that this phenomena is due to some of the parameters in the program, and these parameters will probably have to be further refined by future users of the method.

Viscous Design Verification

The objective of the viscous design verification test was to determine the effect of the viscous corrections on the resulting airfoil shapes at the design stations. For this initial design verification test, the inverse procedure was used at only one span station and only on the upper surface. This seemingly simple case was selected because it poses the most severe test on the program logic. In this case, viscous calculations must be performed on the upper and lower surfaces at all the analysis span stations and on the lower surface of the design station. These viscous results must then be coupled to the outer inviscid calculations properly. In addition, automatic relofting was used in this case in order to generate the design station a closed airfoil.

For this design case, the design station was chosen to be at 0.615 semi-span; and the target pressure distribution is shown on Figure 18. Here the airfoil nose shape was determined by the reloft procedure and the inverse pressures specified on the upper surface for the last eighty percent of the

airfoil. As can be seen, the target distribution has a pressure plateau followed by a gentle recompression and a subsequent almost linear recovery to the trailing edge.

The actual pressures at the design station, which were determined by the method at the end of the computation, are shown on Figure 19. With the exception of the trailing edge point, this distribution is indistinguishable from the target distribution, thus verifying the method. At the trailing edge. the actual pressure coefficient is greater (i.e. more positive) than the target value. The reason for this "discrepency" is very simple. The upper surface designed by the inverse method has a negative slope at the trailing edge, while the lower surface, which was held fixed, has a positive slope. While the effects of boundary layer interaction on the lower surface decrease the effective magnitude of the lower surface slope, they are not sufficient to make it positive. Thus, to satisfy the Kutta condition, the upper surface pressure at the trailing edge has to be more positive than desired.

This phenomena probably can be better understood by considering a strictly inviscid design case. There the flow can leave the upper and lower surfaces either parallel with some positive pressure coefficient or non-parallel with a trailing edge "stagnation pcint". If a design target pressure distribution is used which does not have a rear "stagnation point" and the resultant design surface has non-parallel upper and lower surfaces, the final pressure distribution at the design station will still appear as if the pressures are approaching a rear stagnation point. In other words, the final answers will still correctly reproduce the physics of the problem even if the trailing edge desired pressure was non-physical.

Obviously, this situation has occurred in the present design verification test. However, since this phenomena only affects the last one percent of the design station and the actual design pressure is computed at the end of the calculation, the resultant design is still valid. In addition, it is significant to note that the present method does maintain

the correct physical phenomena and does not permit a user to design a physically unrealistic case.

Figure 20 shows the resultant upper surface displacement thicknesses at the design station. Comparison of this result with those on Figure 16 shows that the boundary layer at the trailing edge of the design station is slightly thicker than those at the other stations, primarily as a result of the difference in the pressure recovery near the trailing edge. In addition, the replacement of the shock wave by a more gentle recovery near the mid-chord of the design station has significantly reduced the sharp increase, or bump, in the displacement thickness near this recovery.

Figure 21 compares the original ONERA M6 airfoil section with the fluid airfoil determined by the inverse procedure at the design station. On the lower surface, where the original airfoil shape was retained, the boundary layer is very thin and viscous effects are obviously small. However, on the upper surface, the new pressure distribution has yielded an effective displacement surface or fluid airfoil of considerably different shape. Notice that the aft portion of the effective airfoil is considerably thicker and the maximum upper surface ordinate occurs further aft near the mid-chord.

As indicated above, after the inverse procedure is completed, a boundary layer calculation is performed for the design surface. The resultant displacement thicknesses are then appropriately subtracted from the fluid airfoil or displacement surface to determine the actual hard airofil to which this fluid airfoil corresponds. Figure 22 compares the original ONERA M6 airfoil with the new design airfoil shape. Since the lower surface was not redesigned in this test, it is identical to the original shape. The upper surface, however, is considerably different in that the aft portion of it is thicker with the maximum thickness near mid chord.

This new shape can be better seen on Figure 23, which shows only the final airfoil corresponding to the target pressure distribution. As can be

seen, the relofting procedure has resulted in a closed trailing edge and different initial nose shape. Also, the new pressure distribution has changed the upper surface shape. Careful examination shows that there is a slight bump in the resultant shape near the mid chord point. This slight, but smooth bump, is a result of the desired pressure recovery between the constant pressure plateau on the forward portion of the airfoil and the near linear recovery on the aft portion of the section. It is believed that this test adequately verifies the present viscous design method and demonstrates that it can yield airfoil shapes which correctly reproduce the target distribution while maintaining the physical fluid dynamics of the problem.

CONCLUSIONS

The direct/inverse transonic wing design method developed during the first phase of this research has been updated to incorporate both viscous and wing/fuselage interference effects into the analysis and design process. The wing relofting procedure developed to enforce trailing edge closure has proven to be effective for both twisted and untwisted wings. However, some method such as optimization needs to be incorporated into the code to provide a means for redesigning the leading edge to obtain the desired flow characteristics in the direct region of the design procedure.

The slender-body approximation of wing-body effects implemented in the design code demonstrated its ability to simulate the first order effect of increasing the span loading at those wing sections external to the fuselage. A more accurate representation of wing-body effects will require an extension of the current potential flow solver to include calculation of the potential flow about the wing-fuselage combination.

The results of the viscous analysis and design verification indicate that the direct/inverse design method presented in this report can be extended to include viscous corrections in the design process. The Nash-Macdonald 2-D strip boundary layer method used to compute the displacement thicknesses for both analysis and design was sufficiently accurate in both

the design and analysis modes for most preliminary design calculations. However, more sophisticated methods such as a 3-D integral method should be implemented in the code if a more detailed representation of the boundary layer is needed.

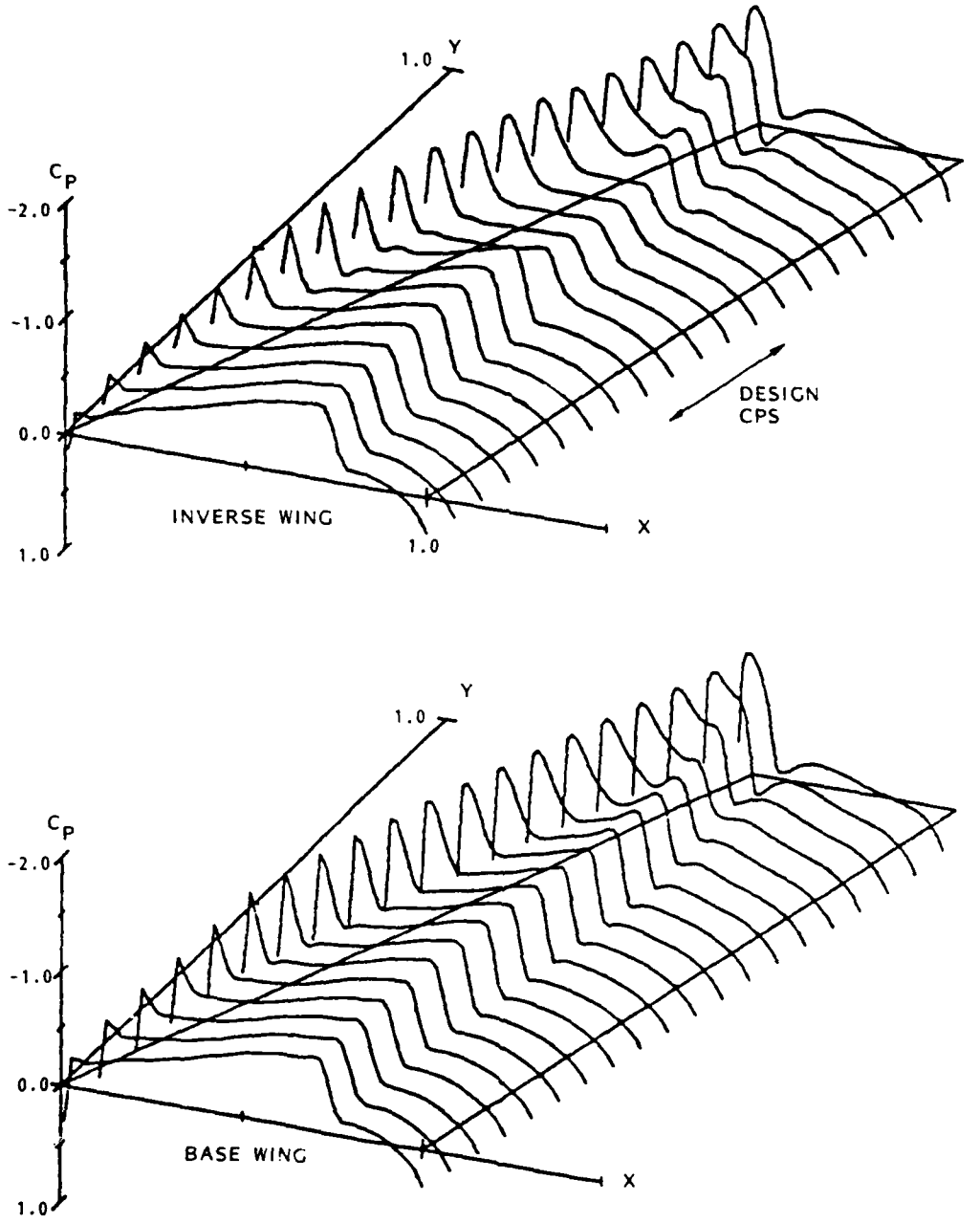

Figure 1. ONERA M6 Base and Target Inverse Pressure Distribution for $M_\infty = 0.84, \alpha = 3.06$

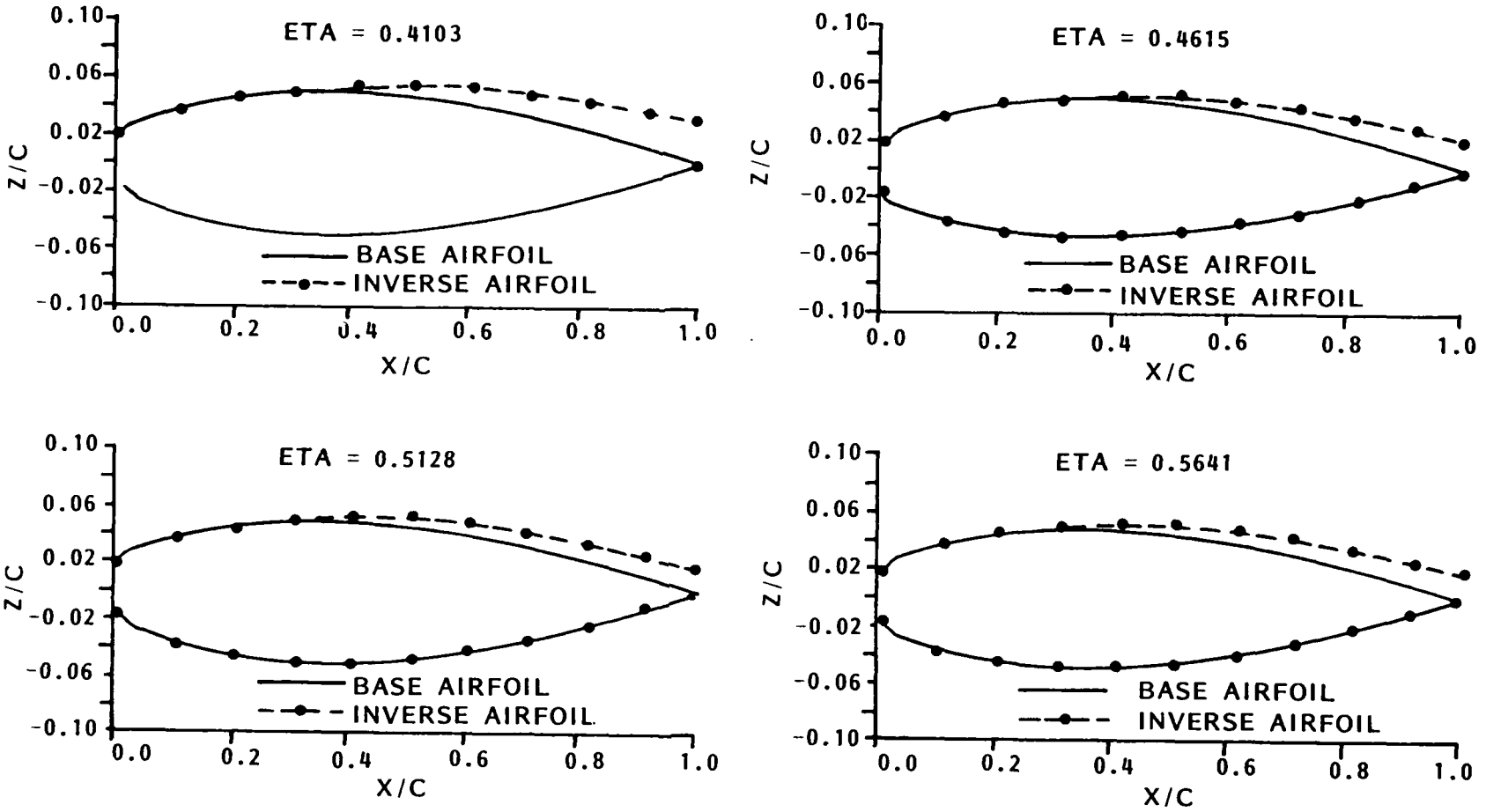

Figure 2. ONERA M6 Inverse Airfoil Shapes without Trailing Edge Closure

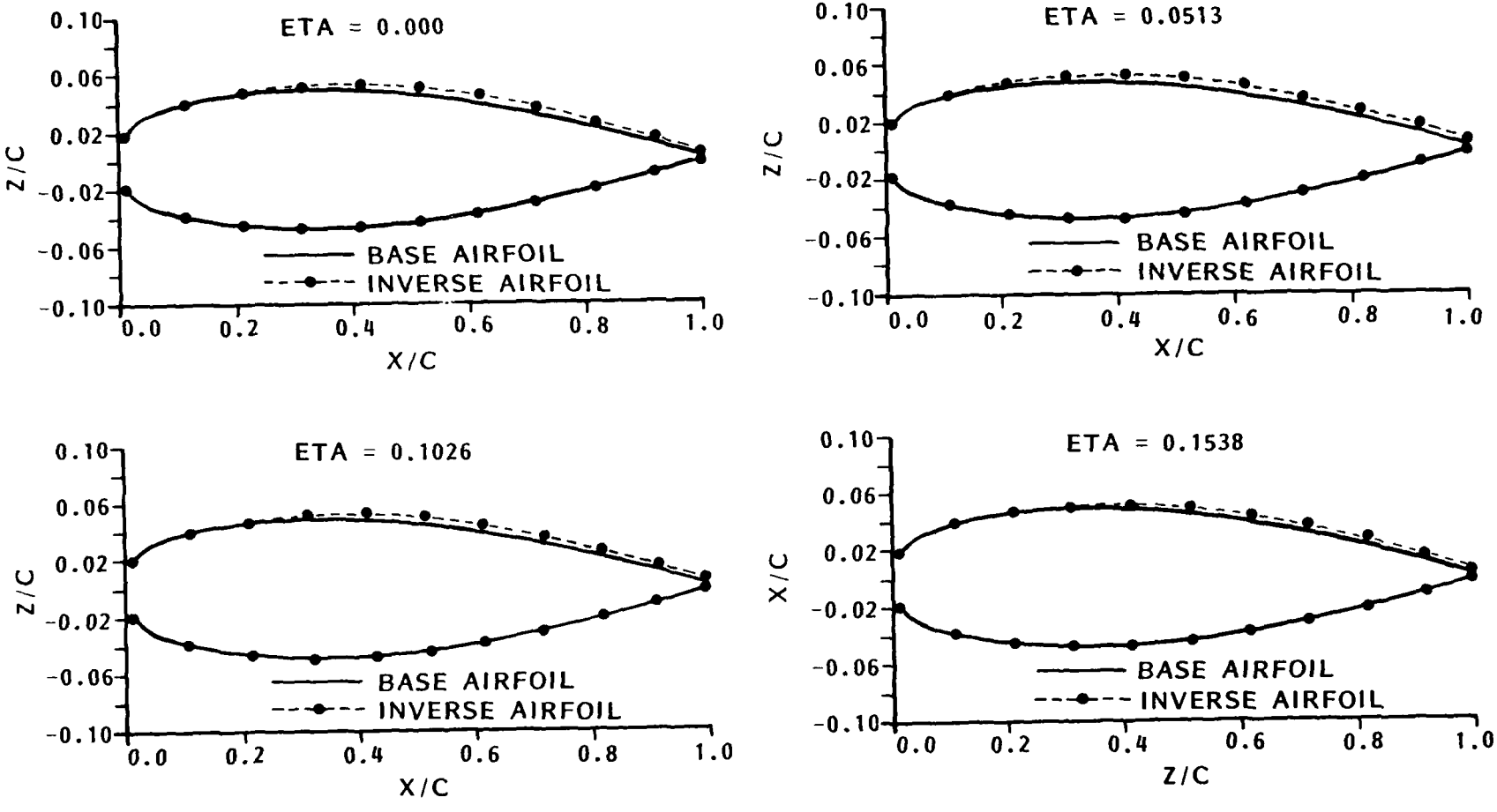

Figure 3. ONERA M6 Inverse Airfoil Shapes with Trailing Edge Closure (Sheet 1 of 5)

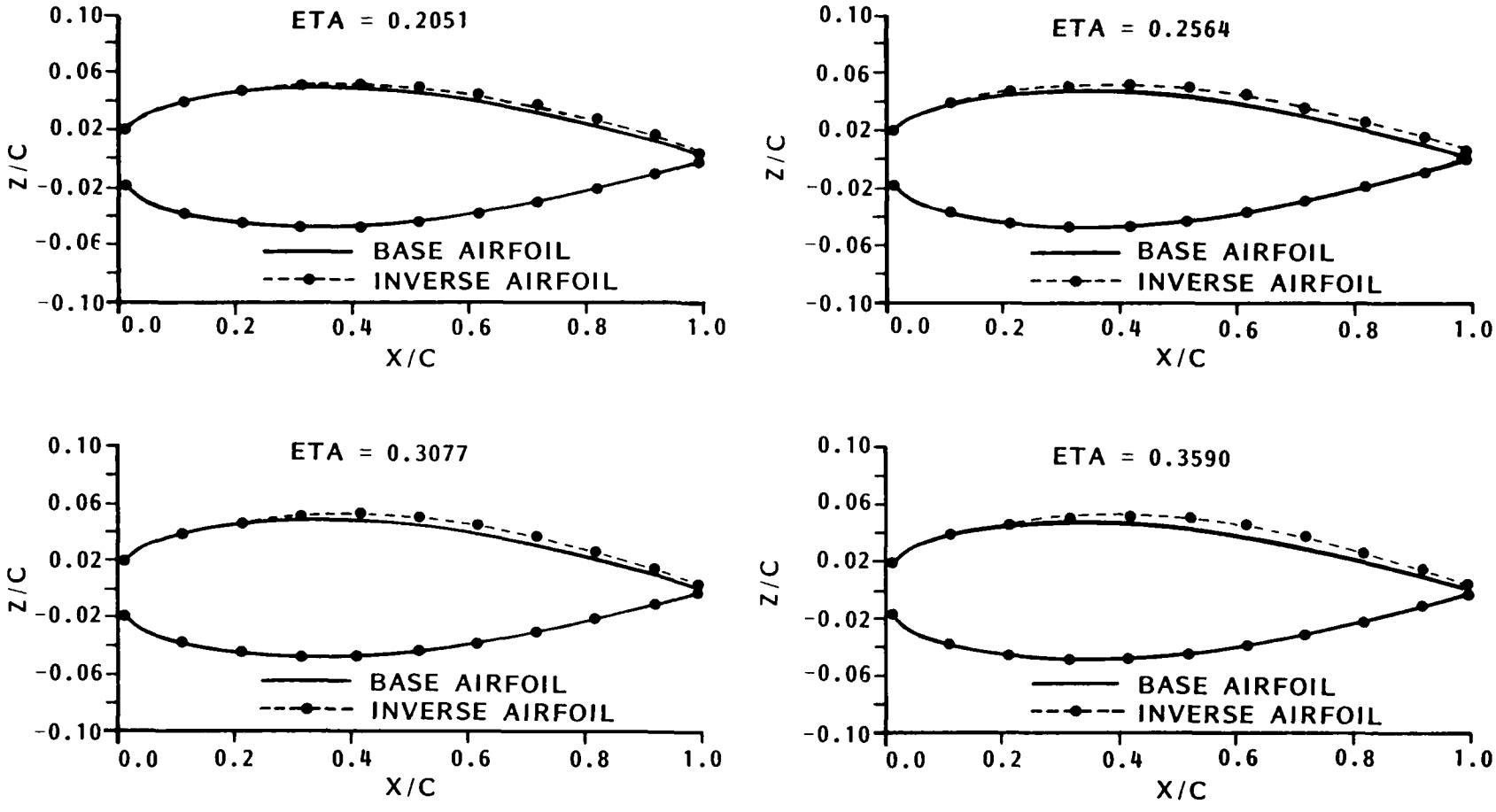

Figure 3. ONERA M6 Inverse Airfoil Shapes with Trailing Edge Closure
(Sheet 2 of 5)

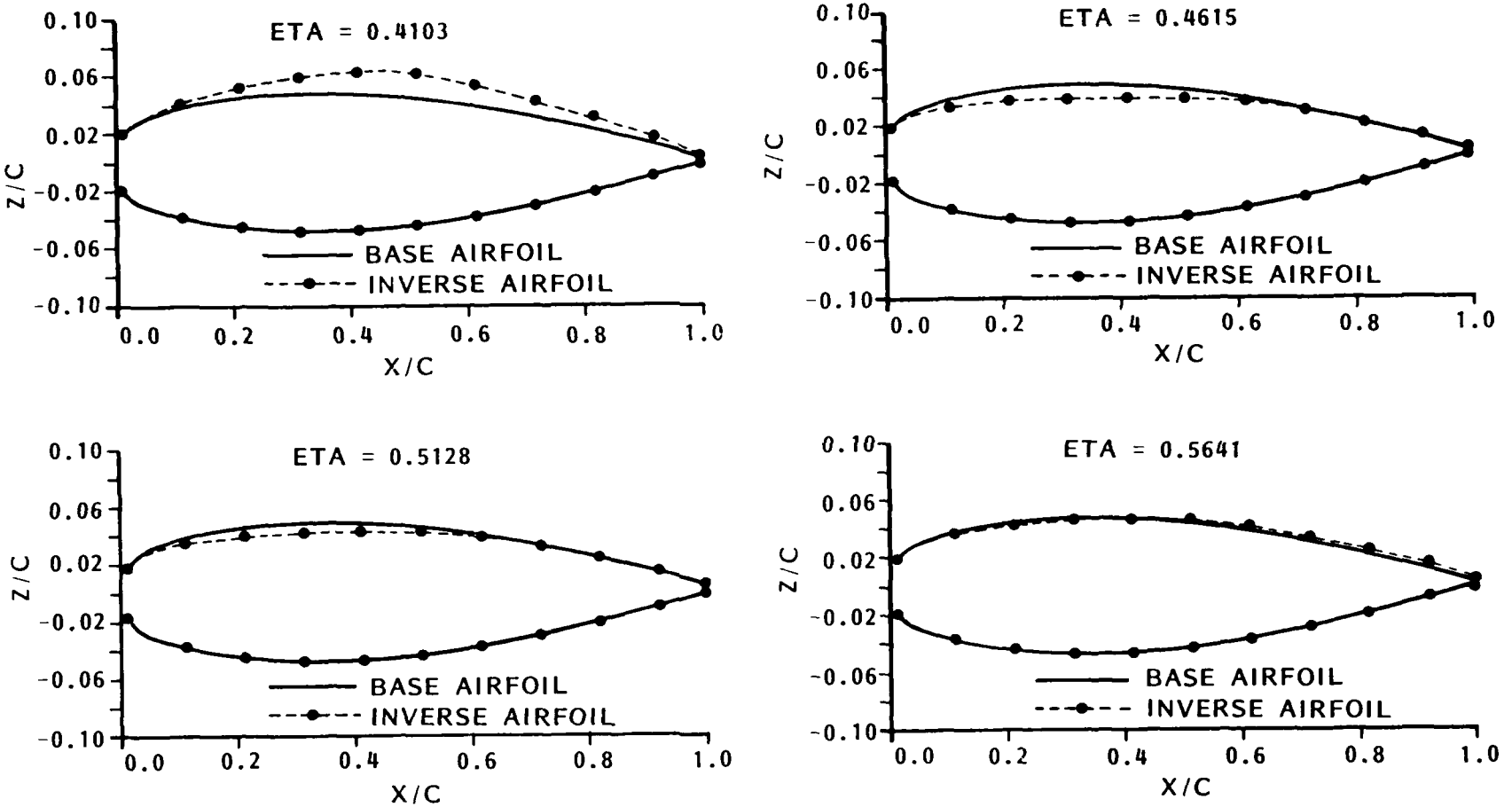

Figure 3. ONERA M6 Inverse Airfoil Shapes with Trailing Edge Closure

(Sheet 3 of 5)

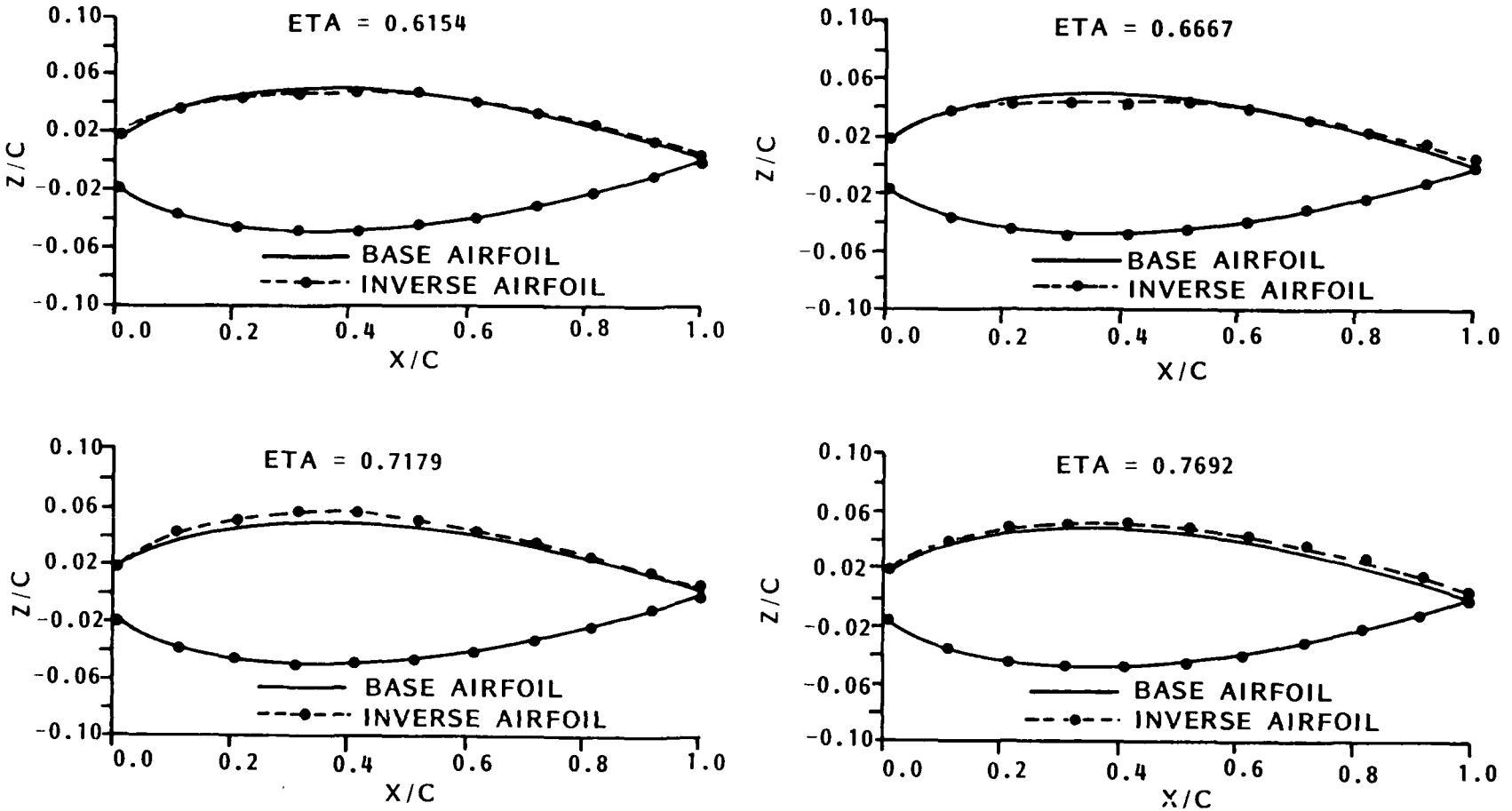

Figure 3. ONERA M6 Inverse Airfoil Shapes with Trailing Edge Closure

(Sheet 4 of 5)

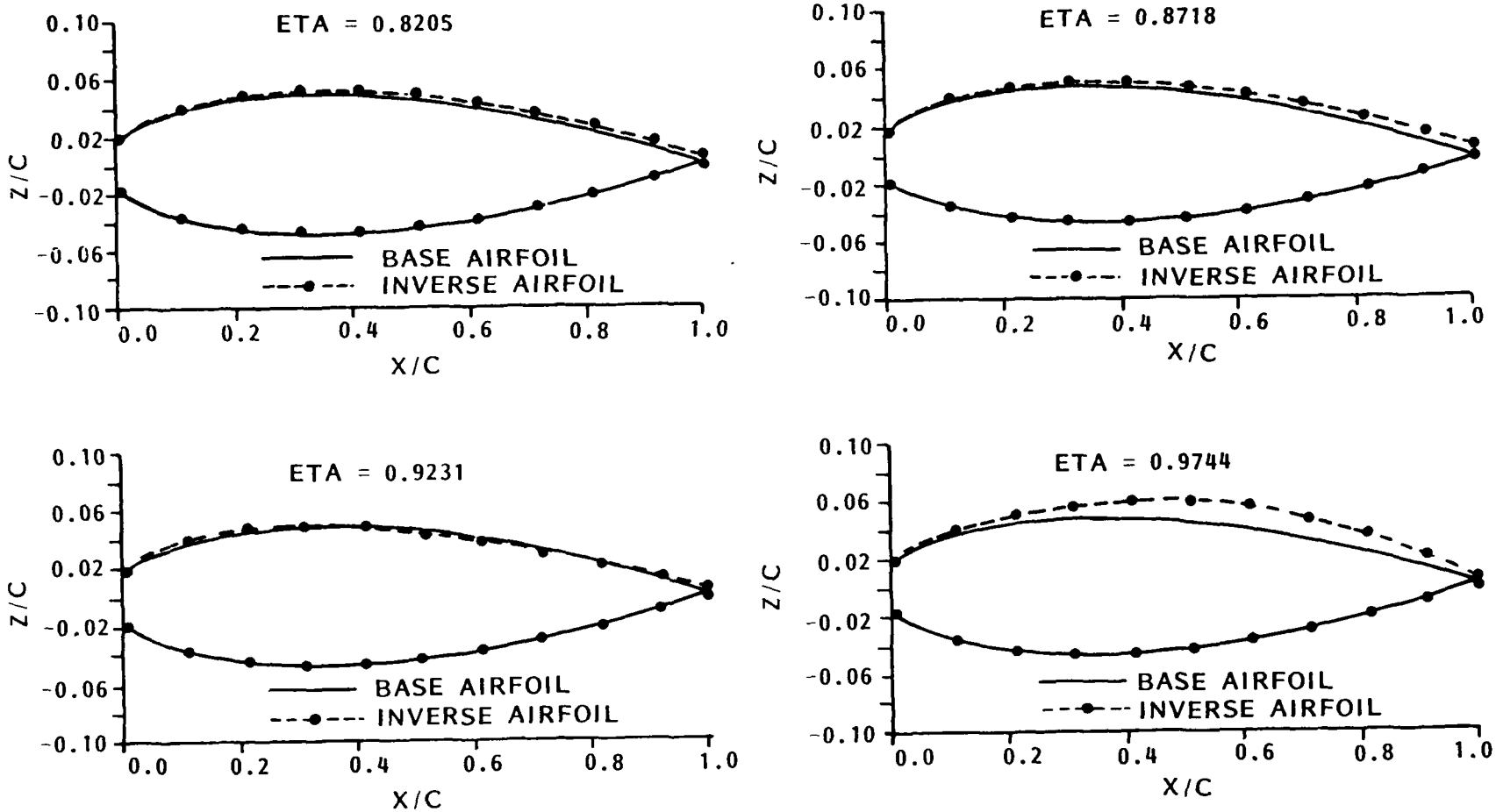

Figure 3. ONERA M6 Inverse Airfoil Shapes with Trailing Edge Closure

(Sheet 5 of 5)

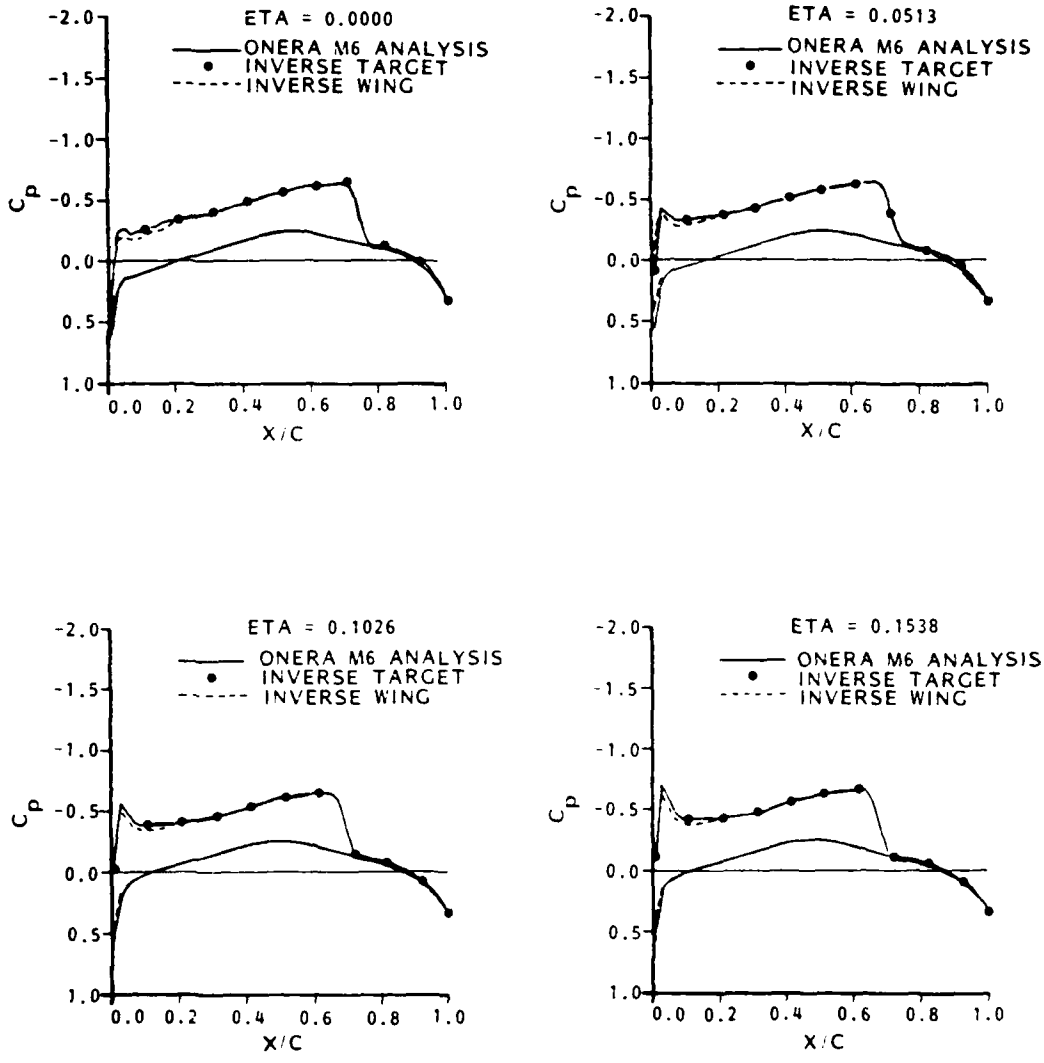

Figure 4. Correlation of Modified ONERA M6 Wing Pressures with Target and Base Wing Pressures at $M_\infty = 0.84$, $\alpha = 3.06$

(Sheet 1 of 5)

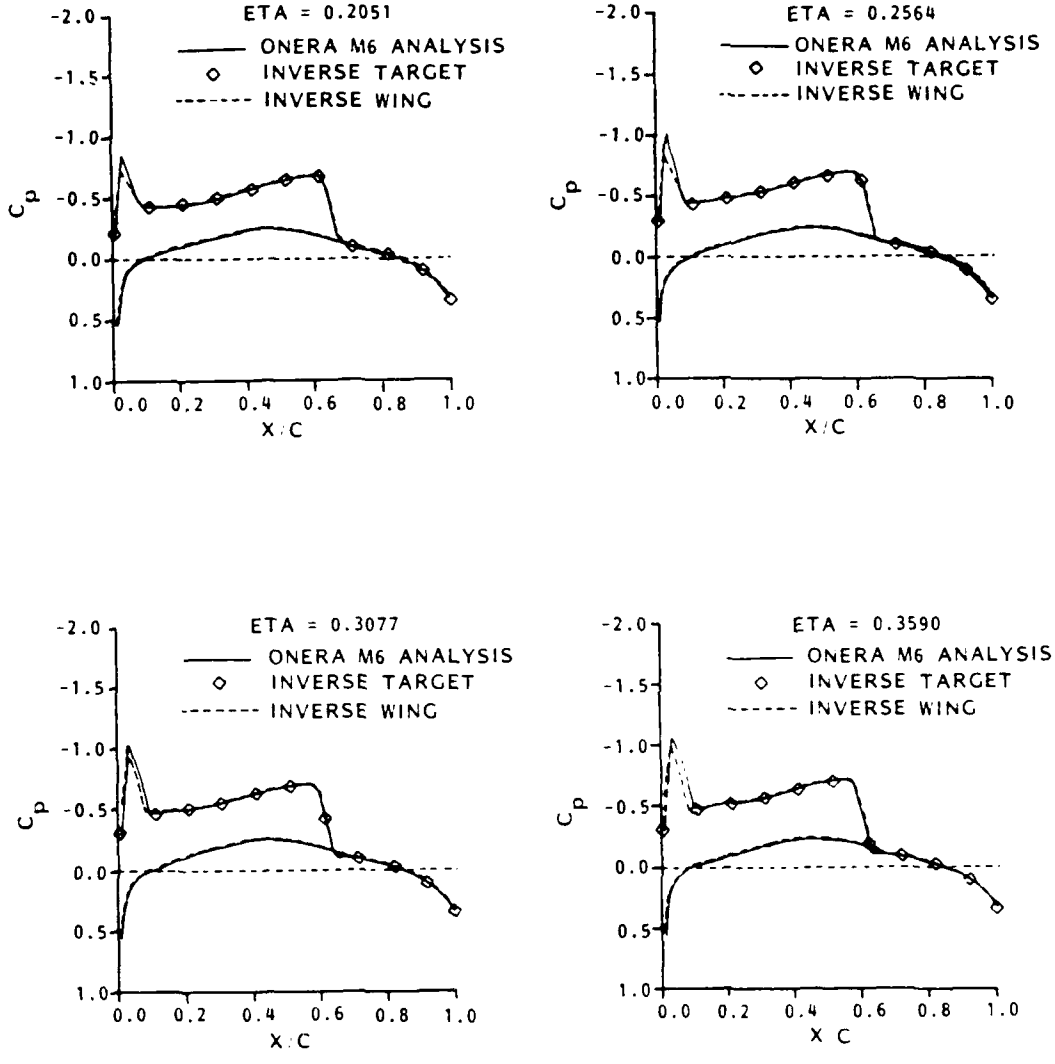

Figure 4. Correlation of Modified ONERA M6 Wing Pressures with Target and Base Wing Pressures at $M\infty = 0.84$, $\alpha = 3.06$
(Sheet 2 of 5)

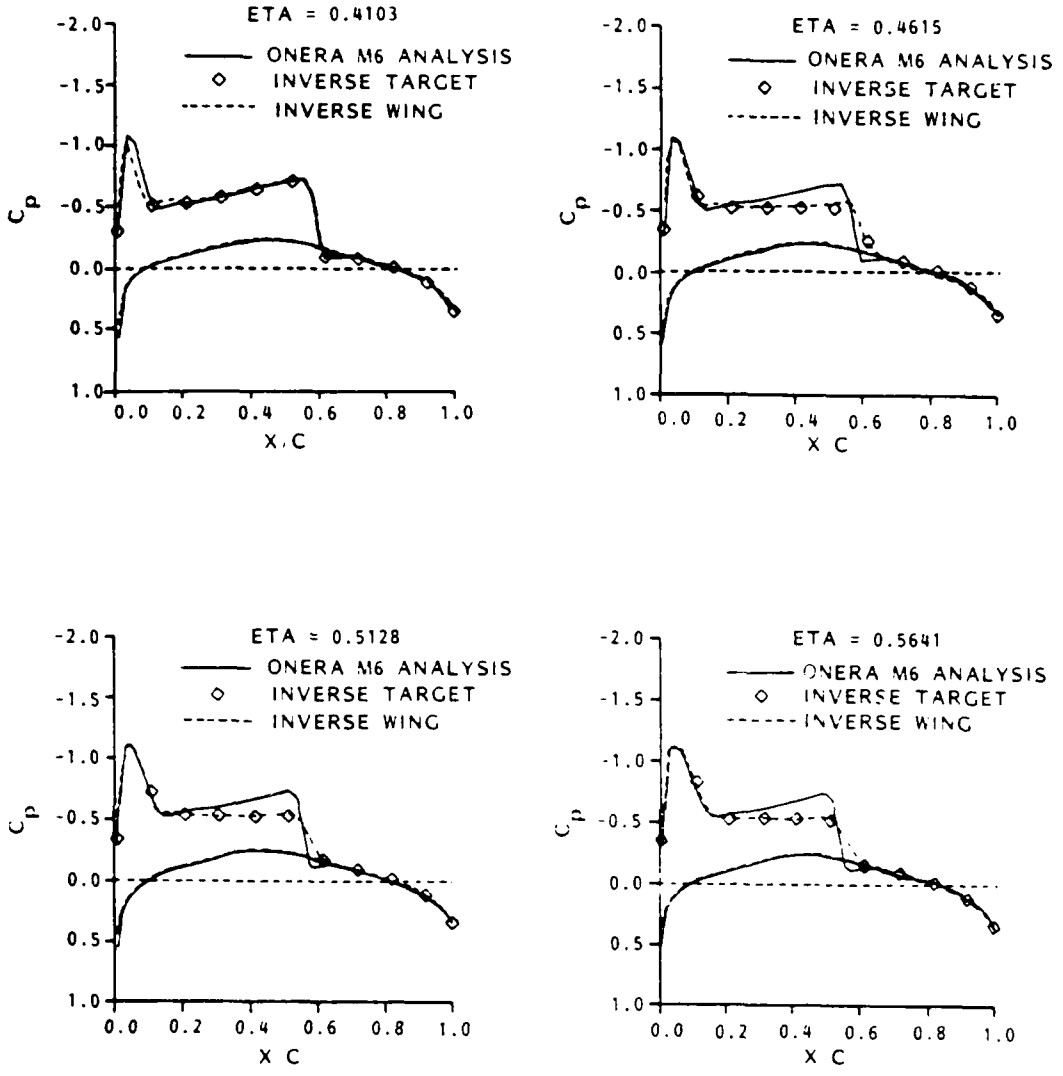

Figure 4. Correlation of Modified ONERA M6 Wing Pressurew with Target and Base Wing Pressures at $M\infty = 0.84$, $\alpha = 3.06$
(Sheet 3 of 5)

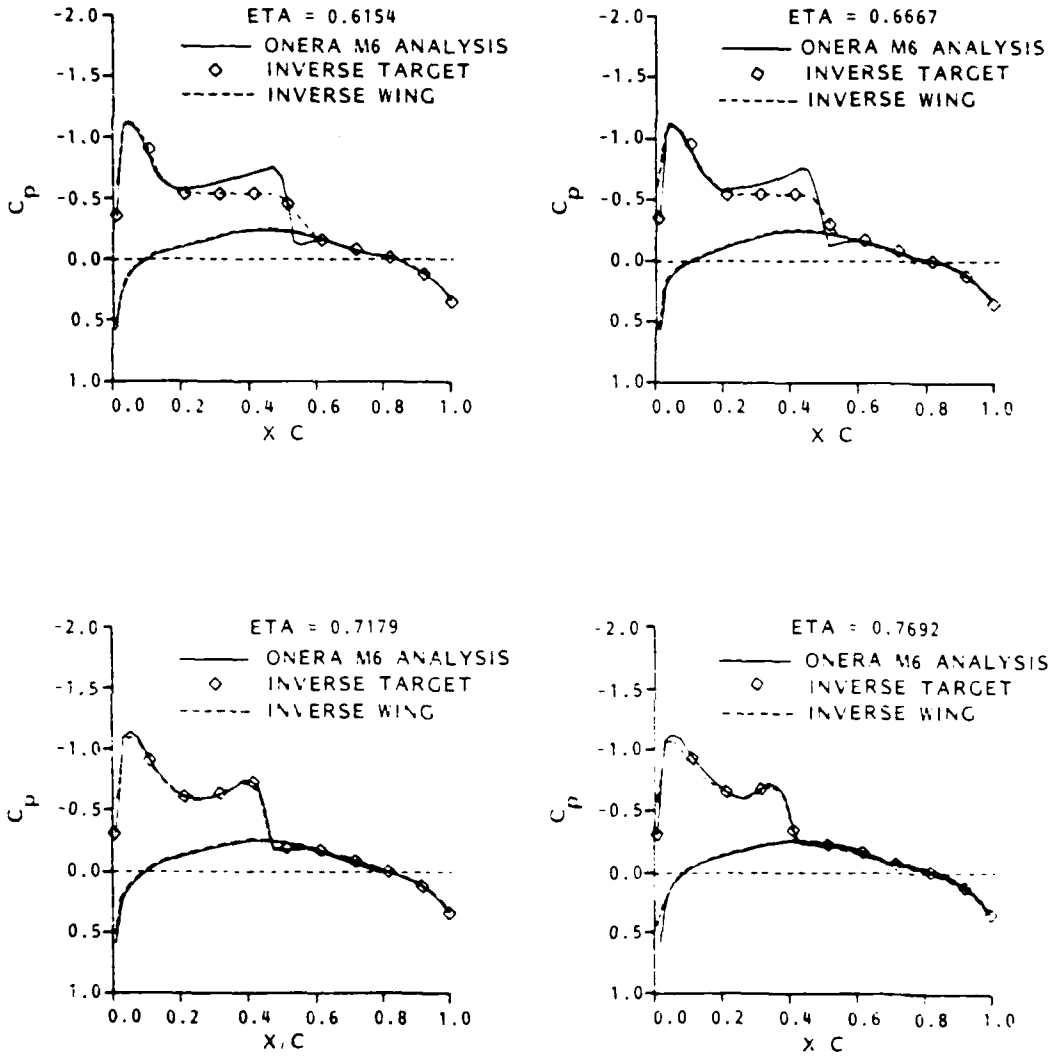

Figure 4. Correlation of Modified ONERA M6 Wing Pressures with Target and Base Wing Pressures at $M\infty = 0.84$, $\alpha = 3.06$

(Sheet 4 of 5)

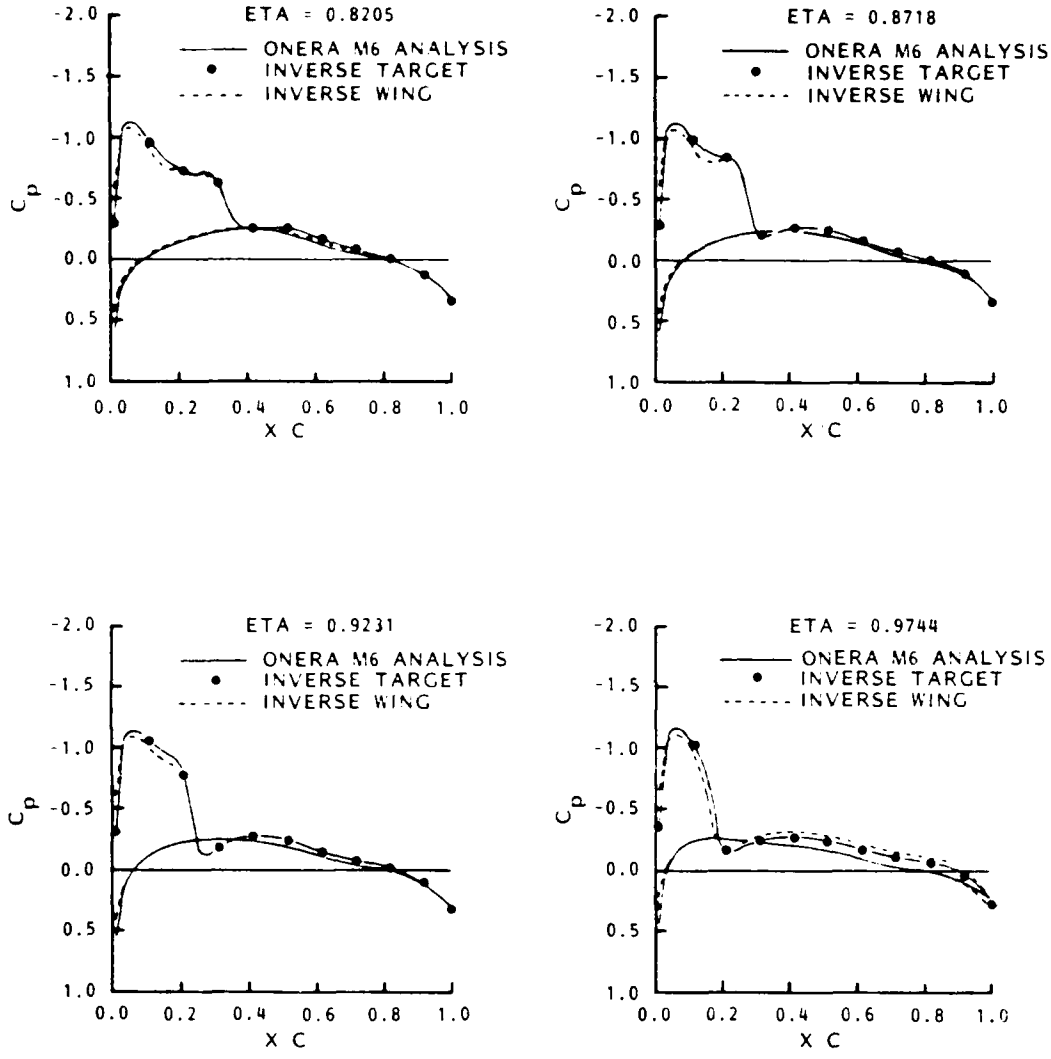

Figure 4. Correlation of Modified ONERA M6 Wing Pressures with Target and Base Wing Pressures at $M_\infty = 0.84$, $\alpha = 3.06$

(Sheet 5 of 5)

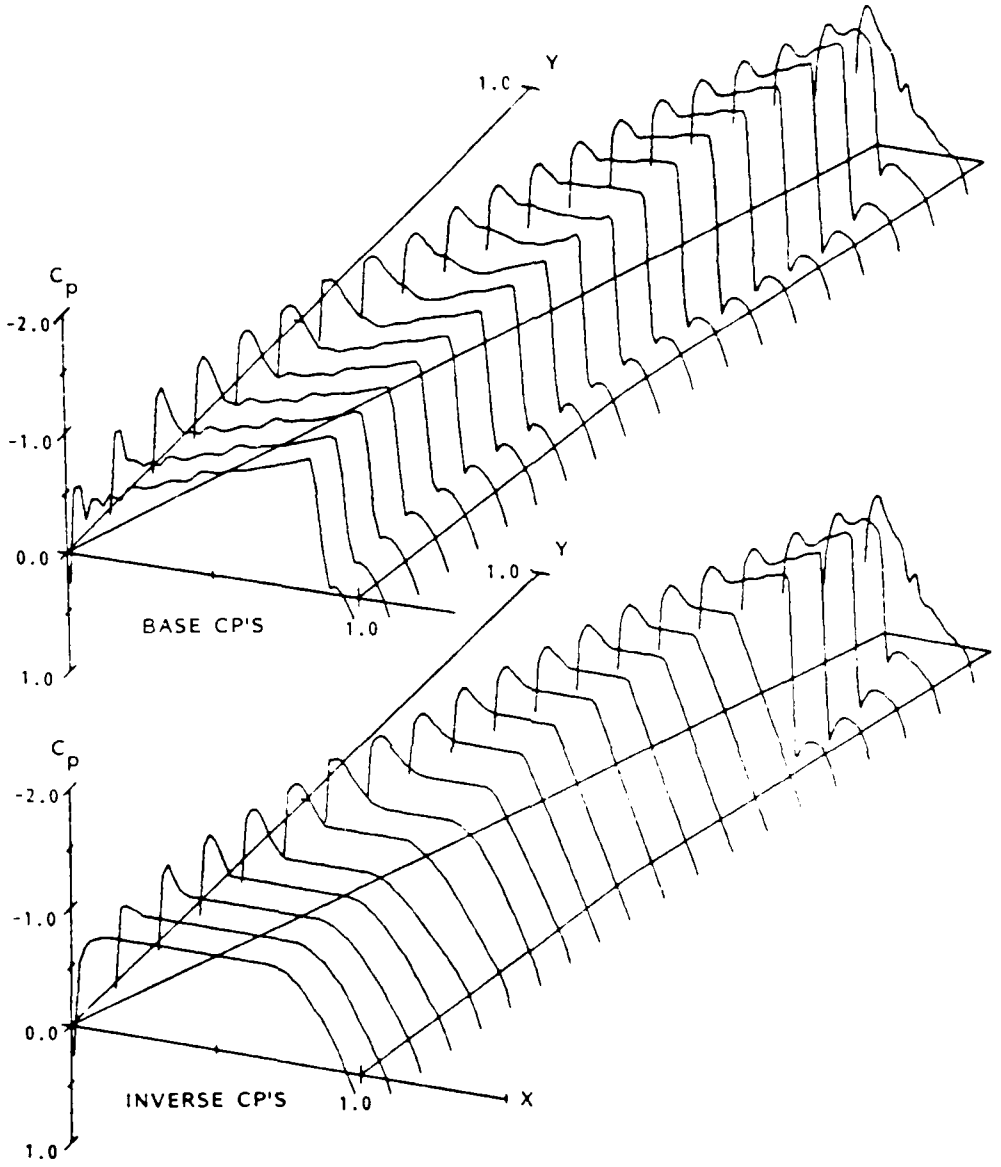

Figure 5. C5A Base and Inverse Target Pressure Distribution at $M_\infty = 0.775, \alpha = 2.0$

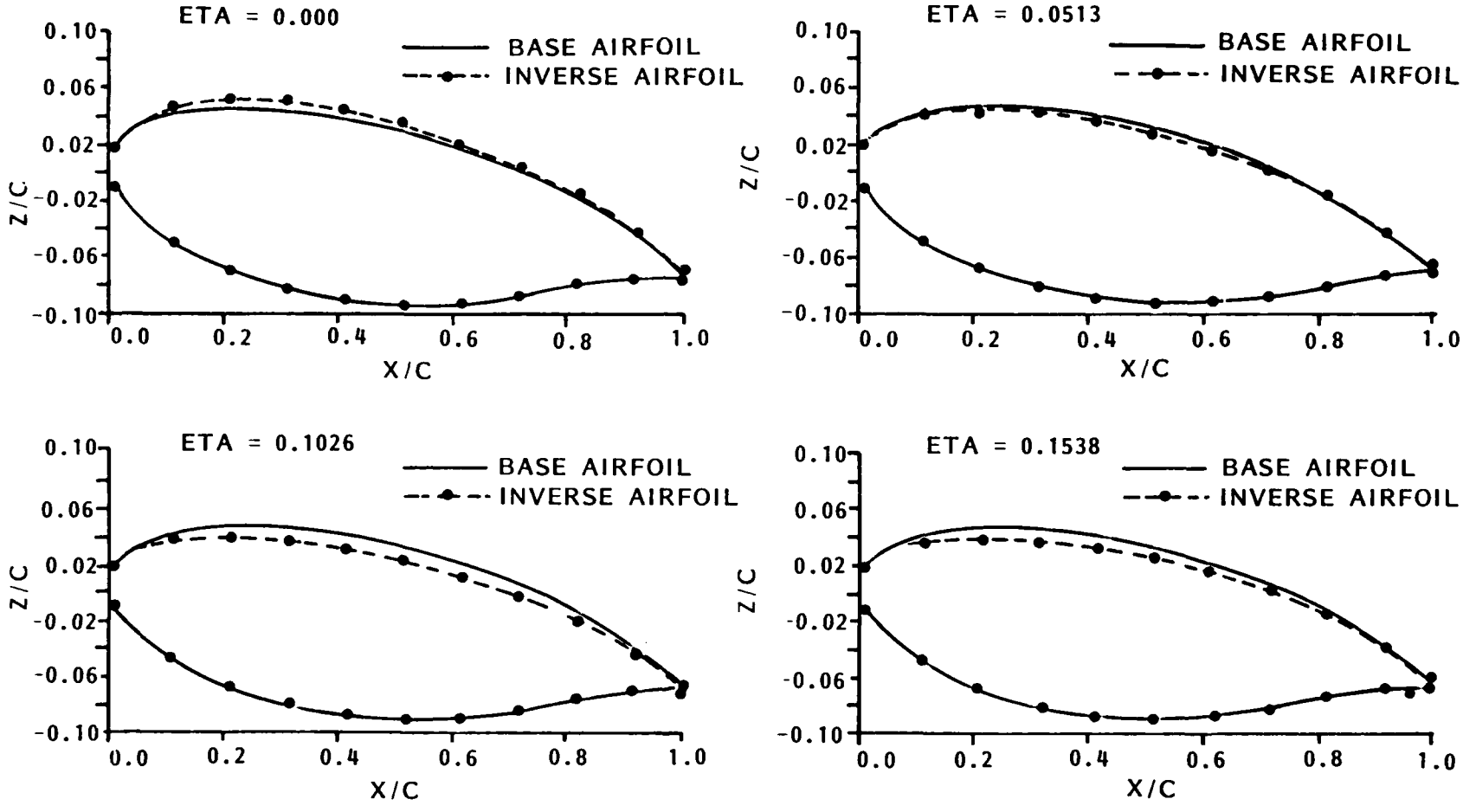

Figure 6. C5A Inverse Airfoil Shapes
(Sheet 1 of 4)

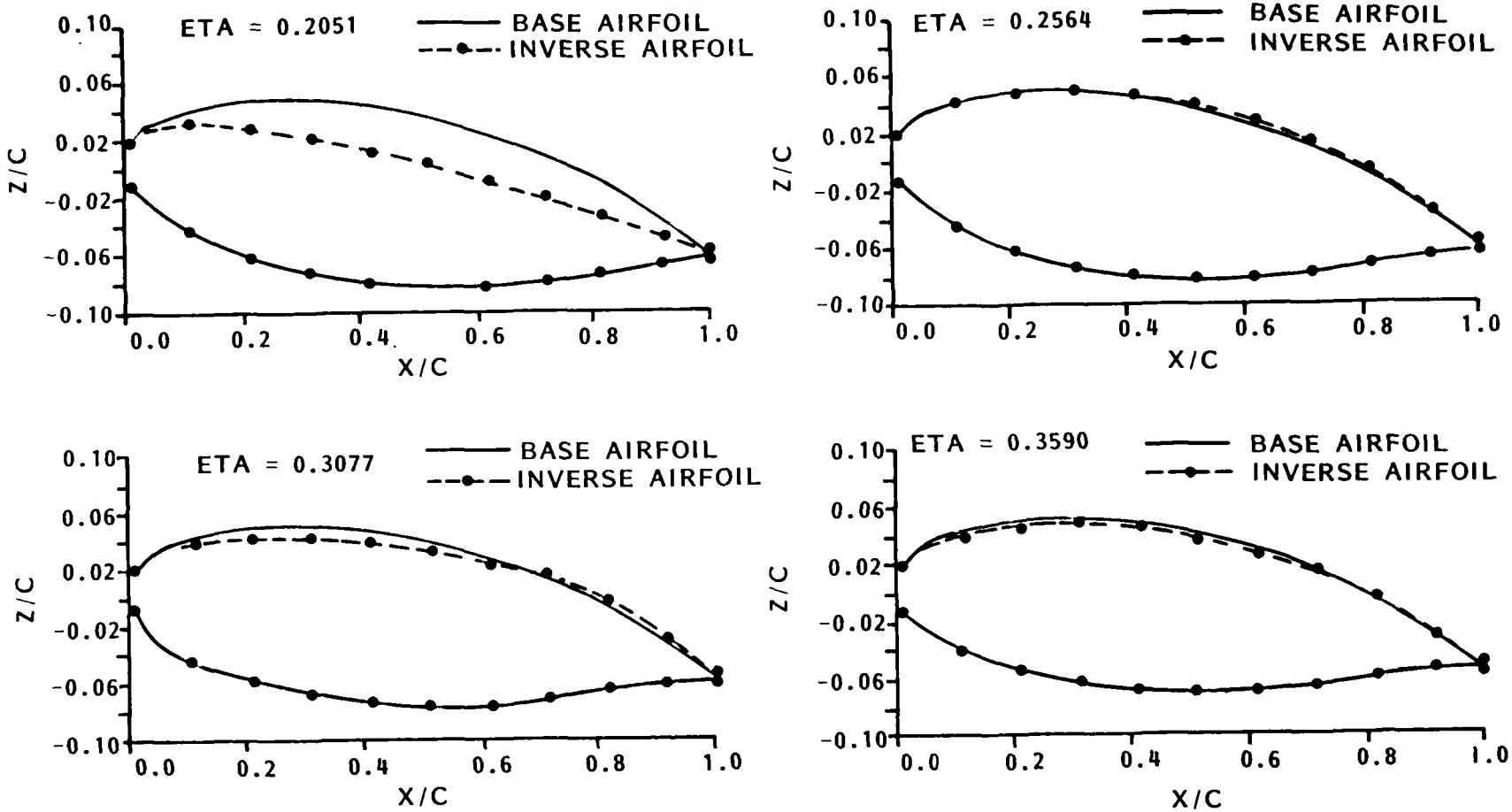

Figure 6. C5A Inverse Airfoil Shapes
(Sheet 2 of 4)

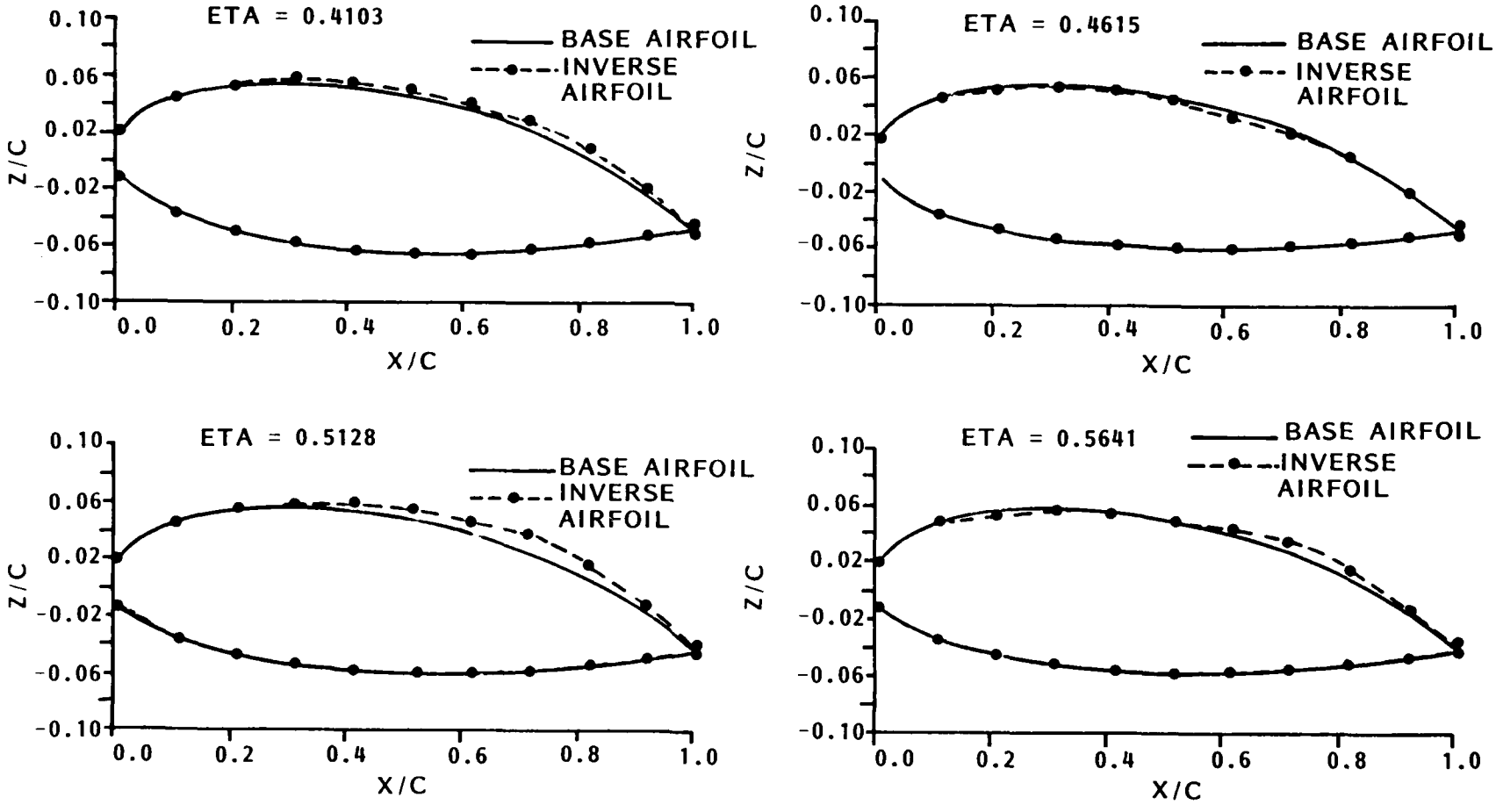

Figure 6. C5A Inverse Airfoil Shapes
(Sheet 3 of 4)

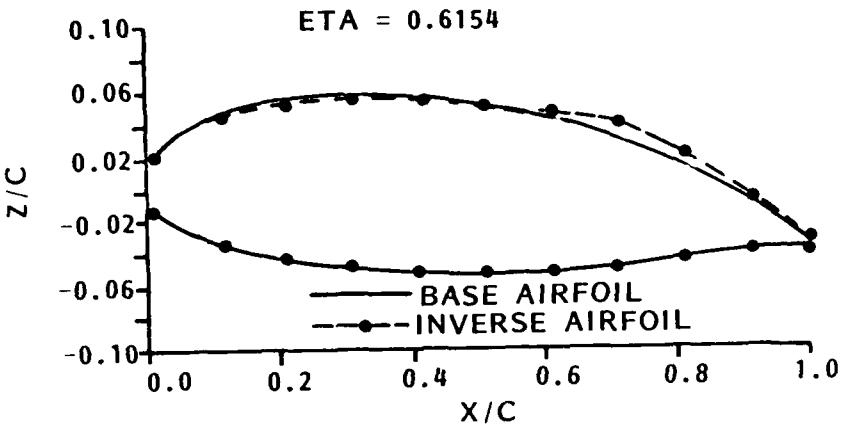

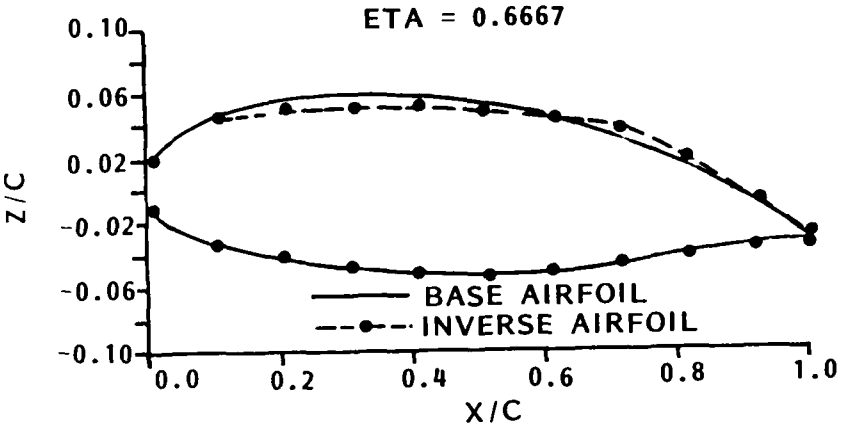

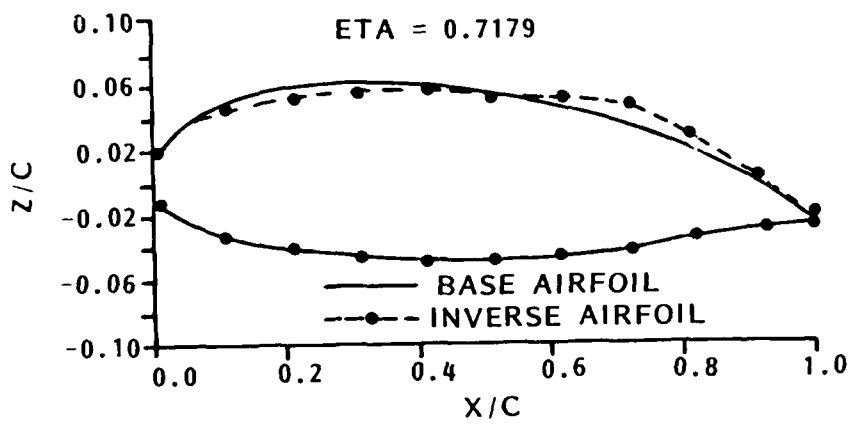

Figure 6. C5A Inverse Airfoil Shapes

(Sheet 4 of 4)

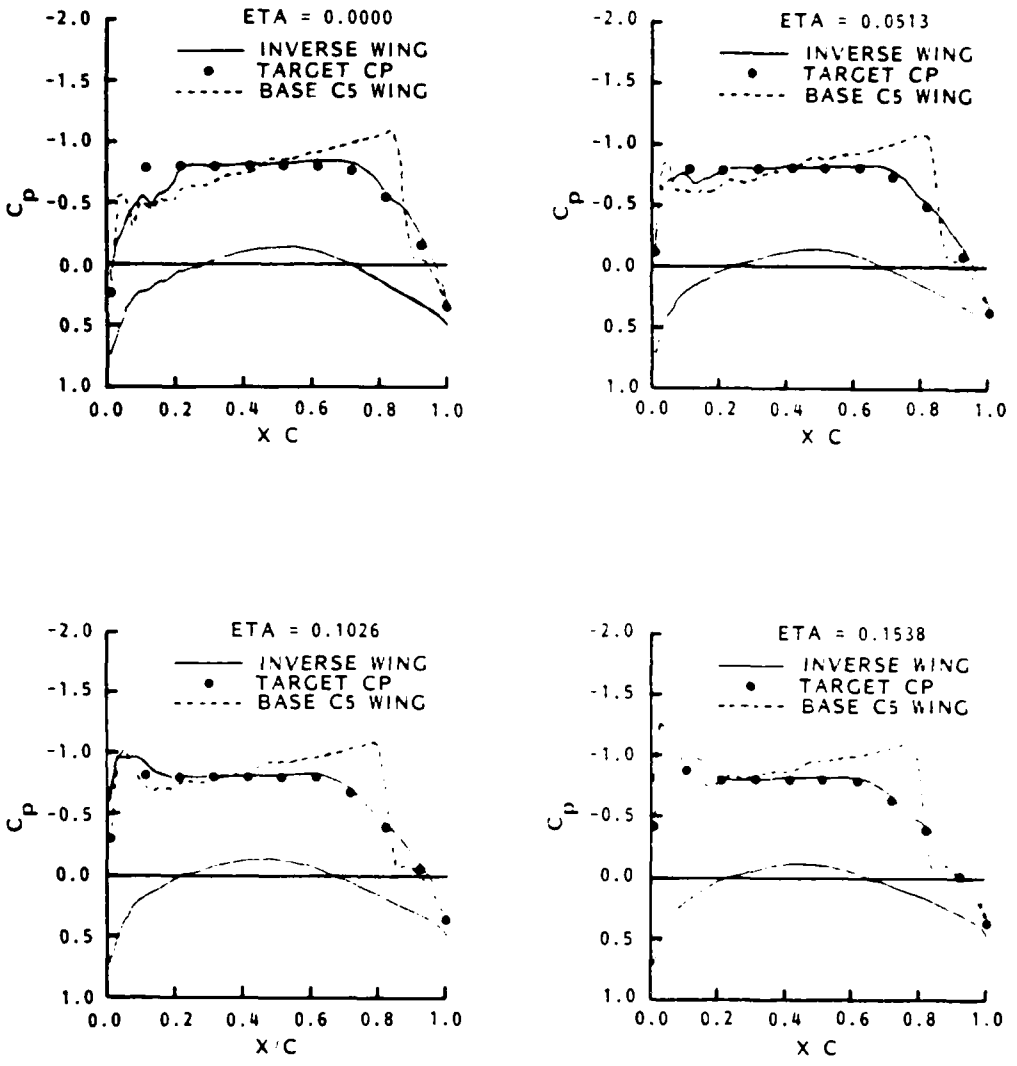

Figure 7. Correlation of Modified C5A Pressures with Target and Base Wing Pressures at $M_\infty = 0.775$, $\alpha = 2.0$

(Sheet 1 of 4)

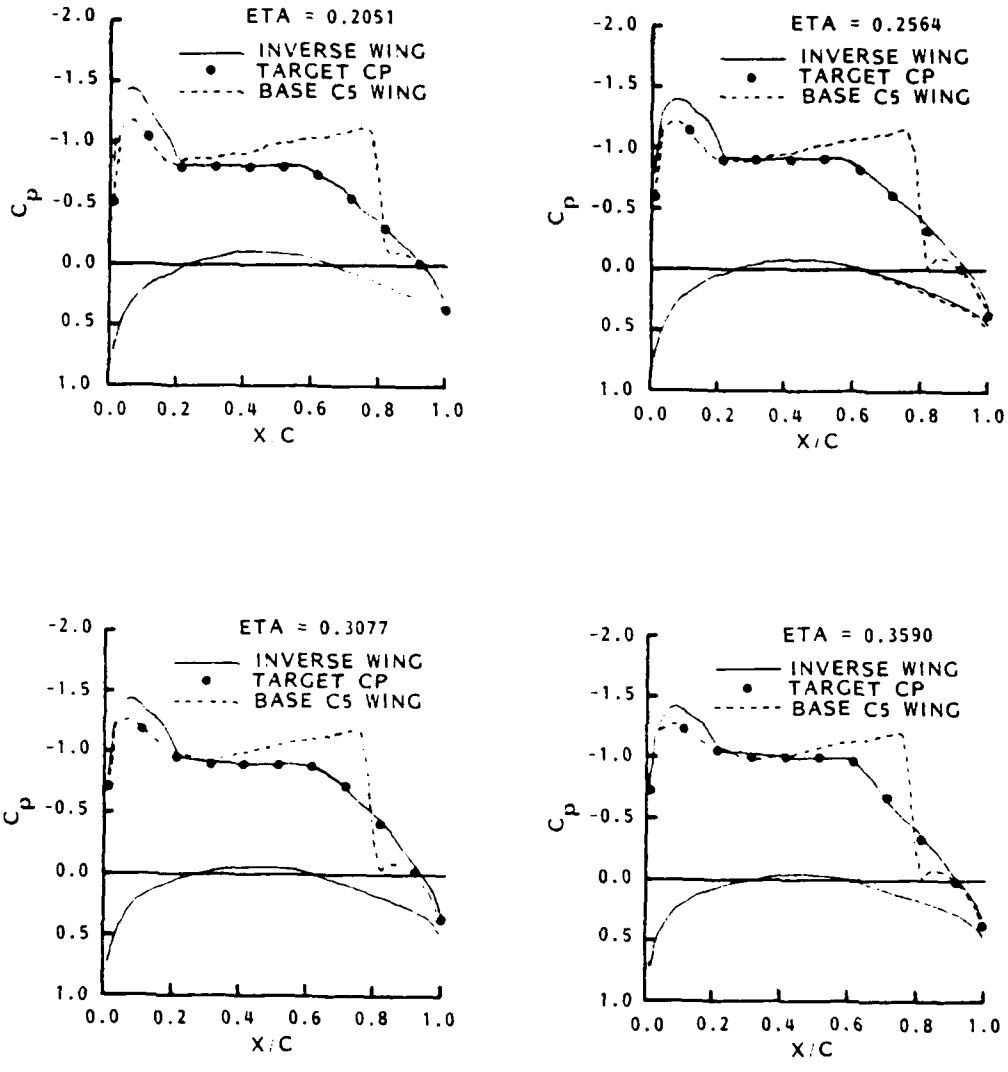

Figure 7. Correlation of Modified C5A Pressures with Target and Base Wing Pressures at $M_\infty = 0.775$, $\alpha = 2.0$
(Sheet 2 of 4)

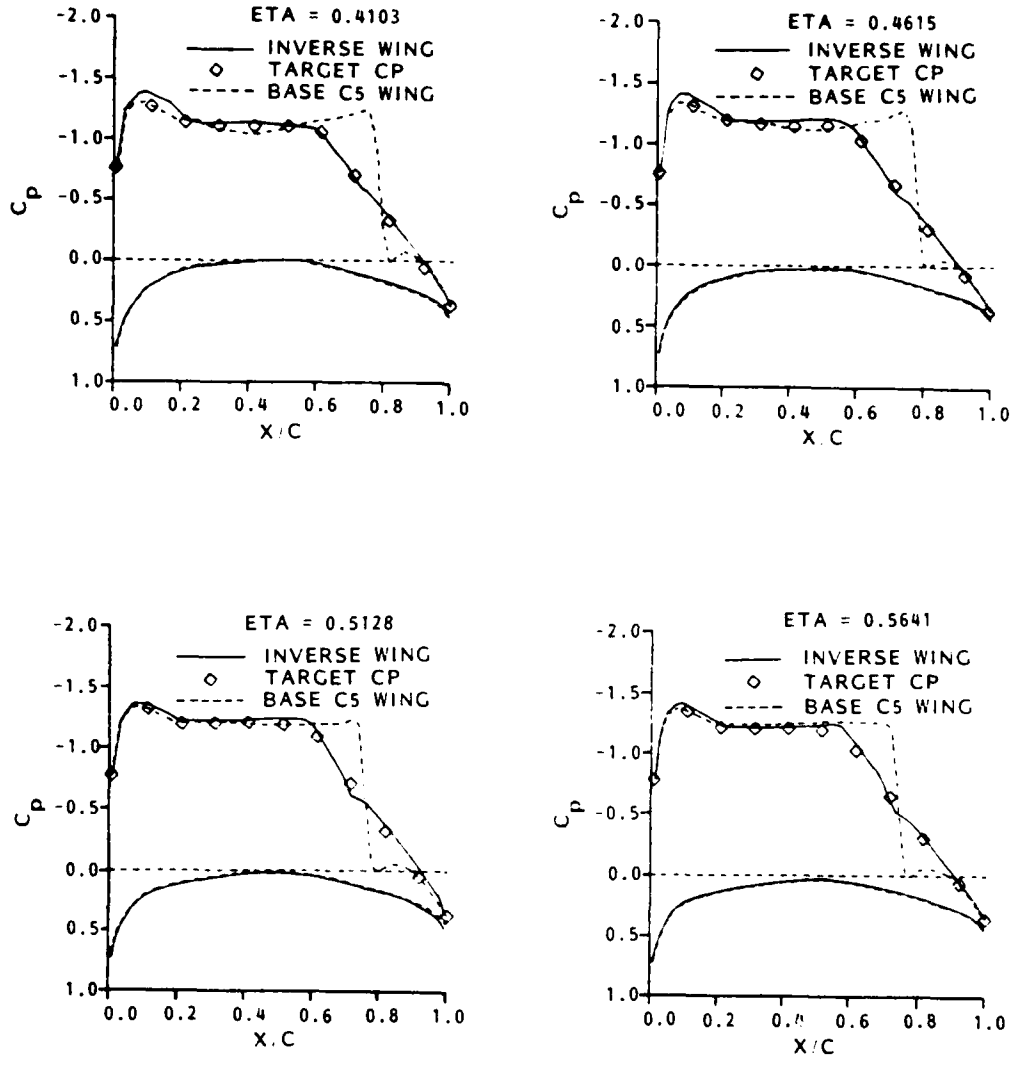

Figure 7. Correlation of Modified C5A Pressures with Target and Base Wing Pressures at $M_\infty = 0.775$, $\alpha = 2.0$
(Sheet 3 of 4)

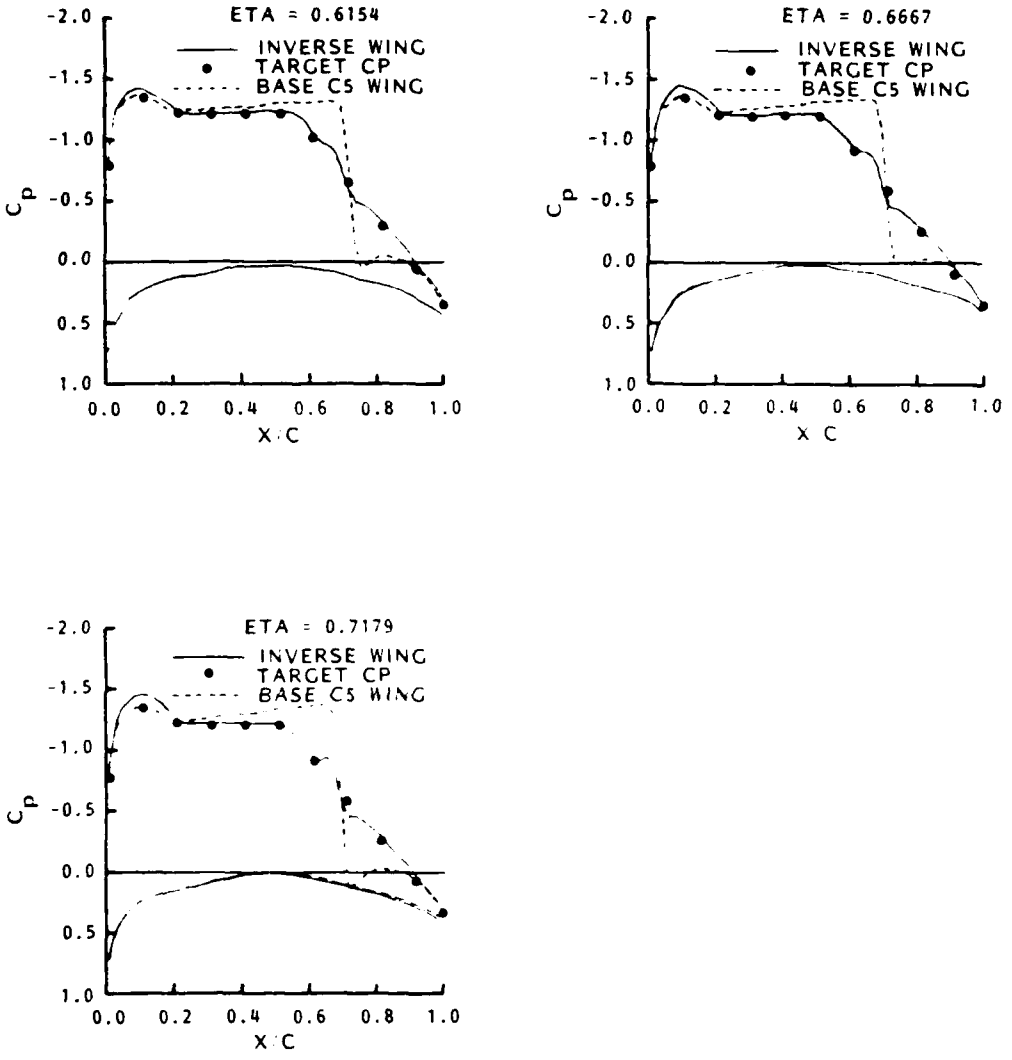

Figure 7. Correlation of Modified C5A Pressures with Target and Base Wing Pressures at $M_\infty = 0.775$, $\alpha = 2.0$

(Sheet 4 of 4)

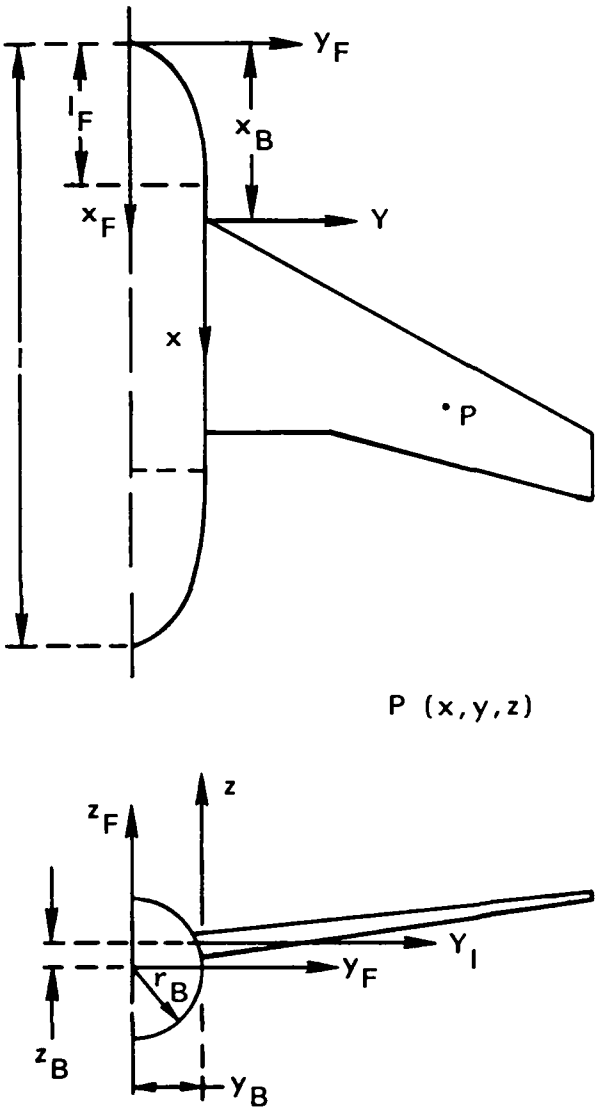

POINT P:

$x_F = x_B + x$

$y_F = y_B + y$

$z_F = z_B + z$

x_B = XBODY

y_B = YBODY

z_B = ZBODY

r_B = RBODY

l = LENGTH

l_F = ALF

Figure 8. Fuselage Nomenclature

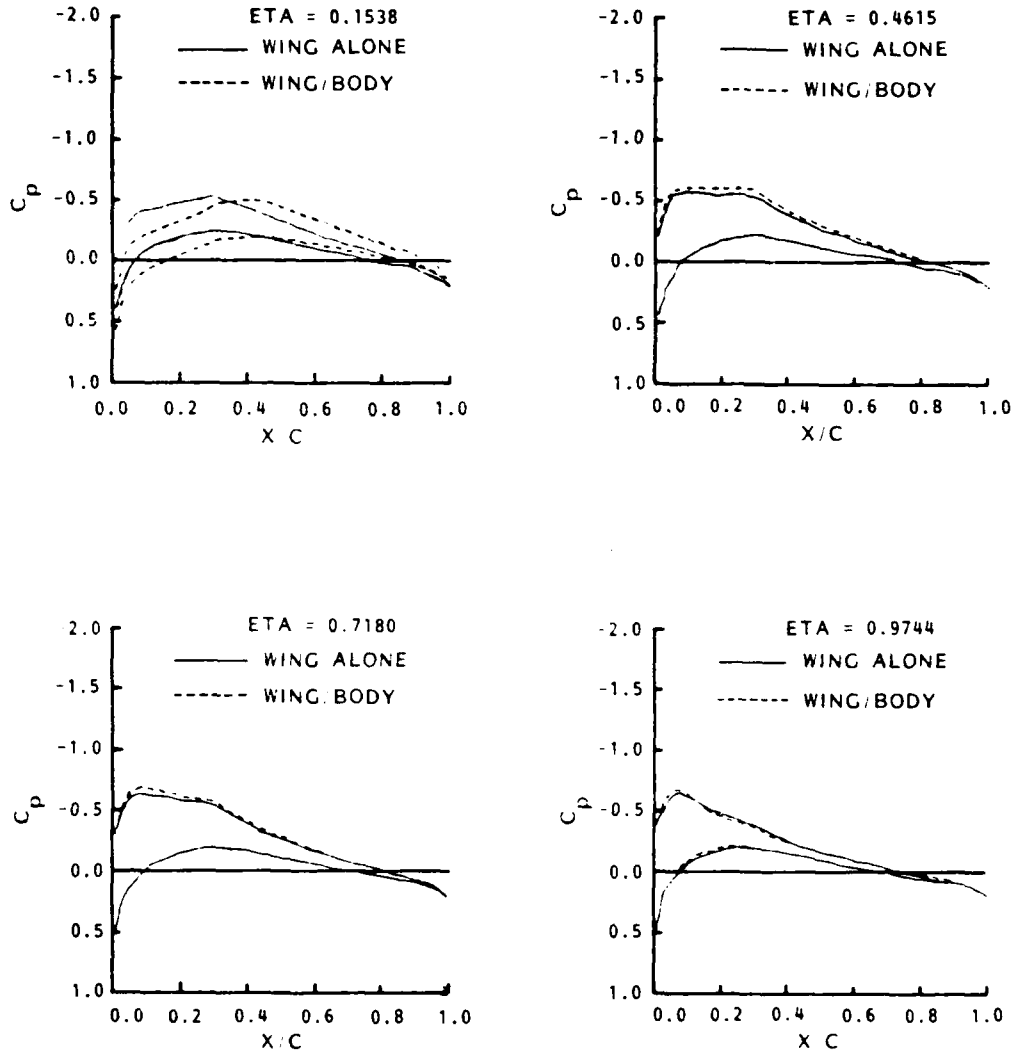

Figure 9. RAE Wing "A" Wing Alone vs Wing/Body Pressure Distribution at $M\infty = 0.80$, $\alpha = 2.0$

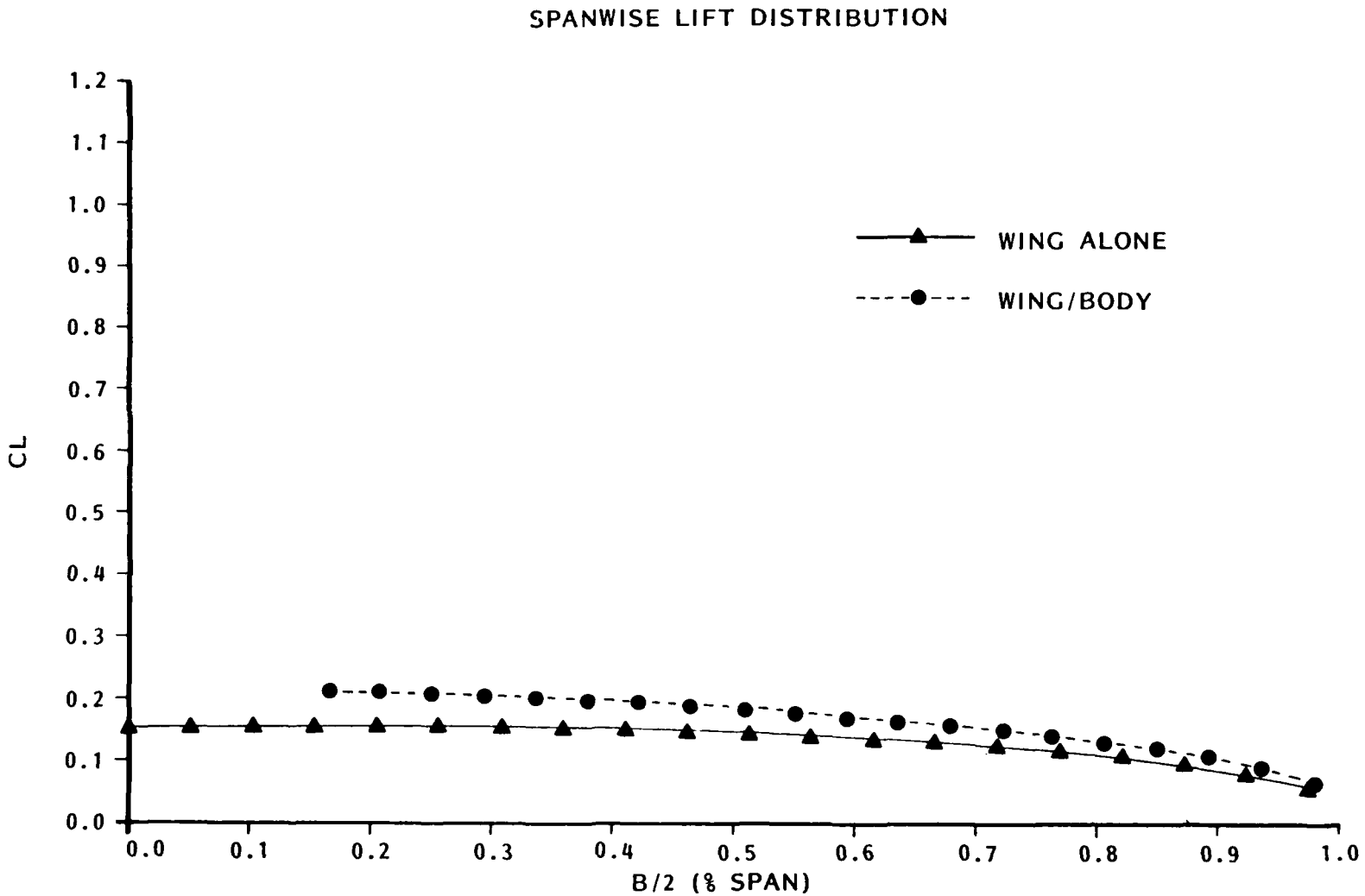

Figure 10. RAE Wing Alone vs Wing/Body Semi-span Loading

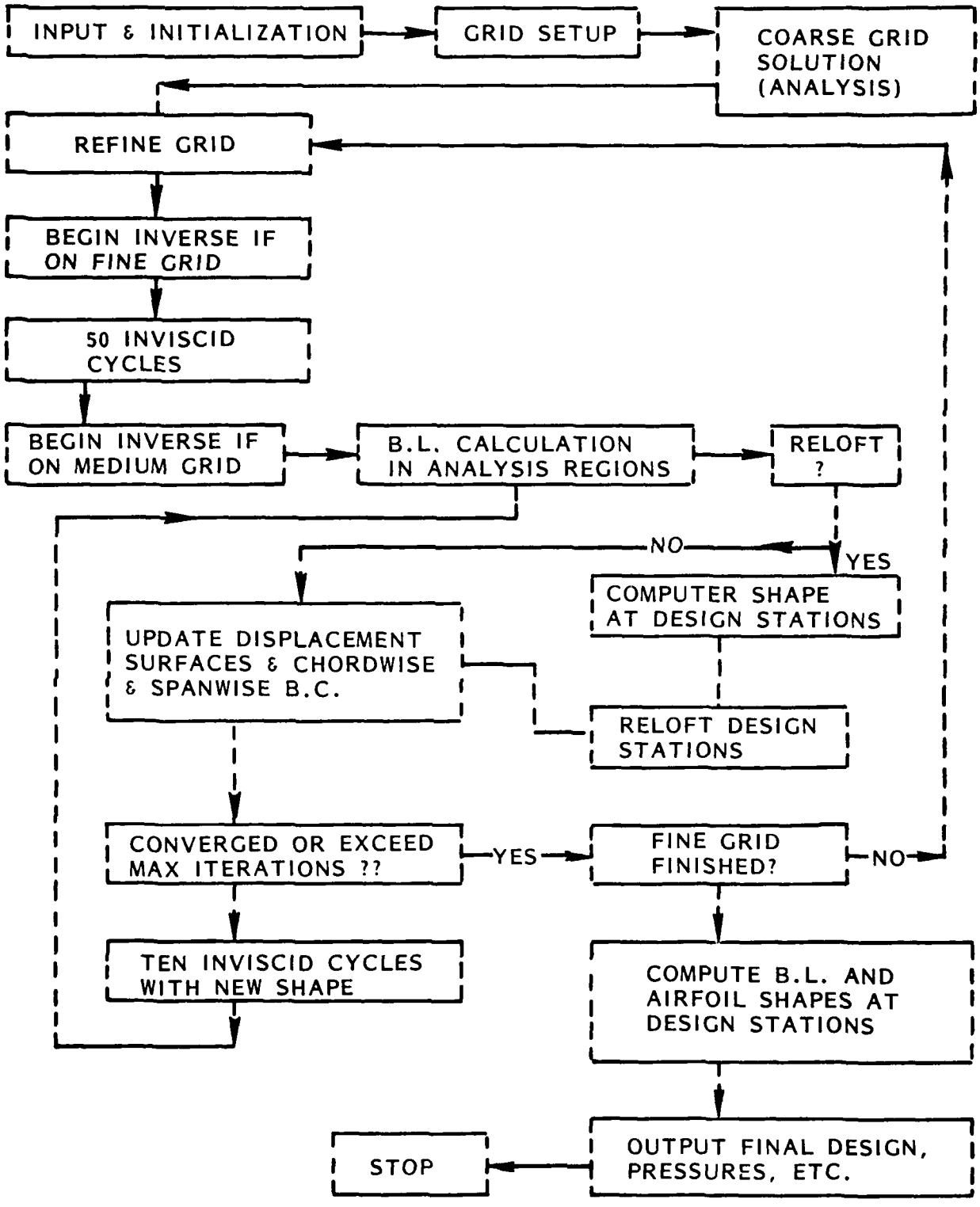

Figure 11. Viscous Design and Relofting Procedure

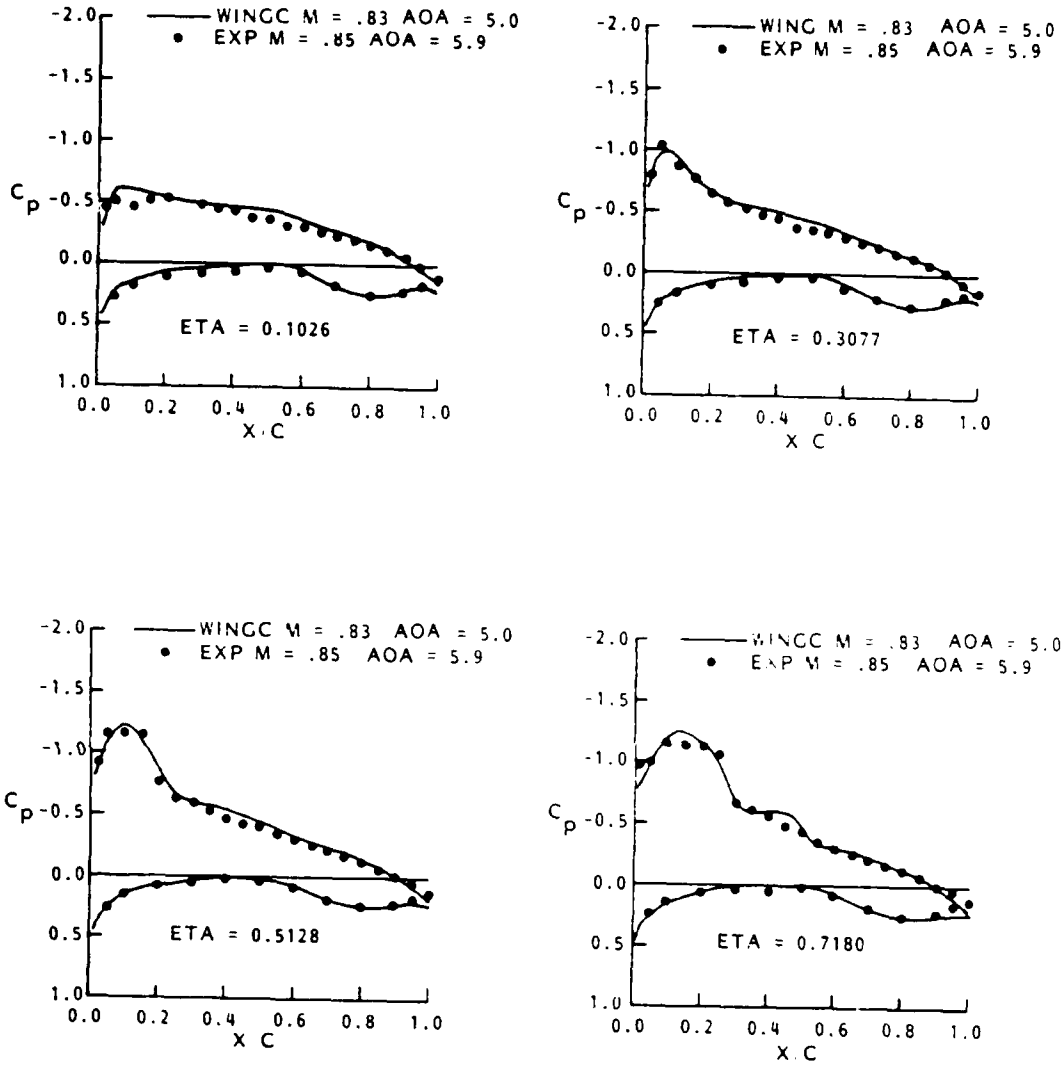

Figure 12. Correlation of WING C Analysis and Experimental Pressure Coefficients at $M_\infty = 0.83$, $\alpha = 5.0$
(Sheet 1 of 2)

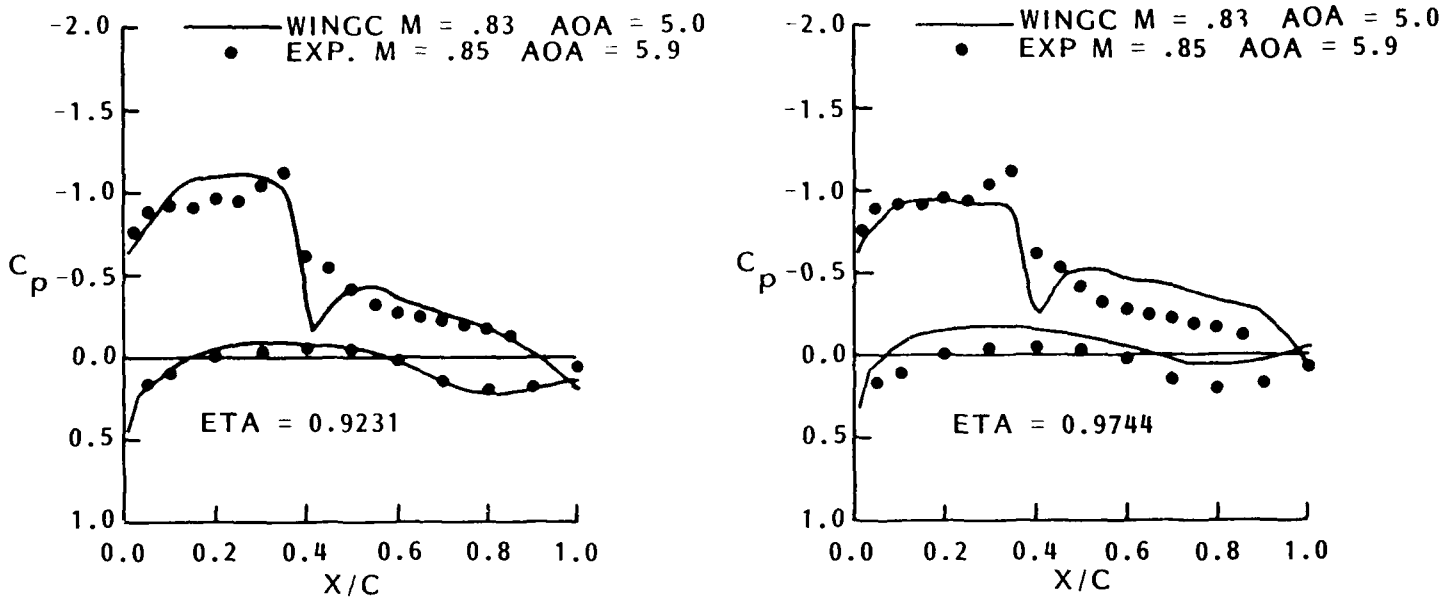

Figure 12. Correlation of WING C Analysis and Experimental Pressure Coefficients at $M\infty = 0.83$, $\alpha = 5.0$
(Sheet 2 of 2)

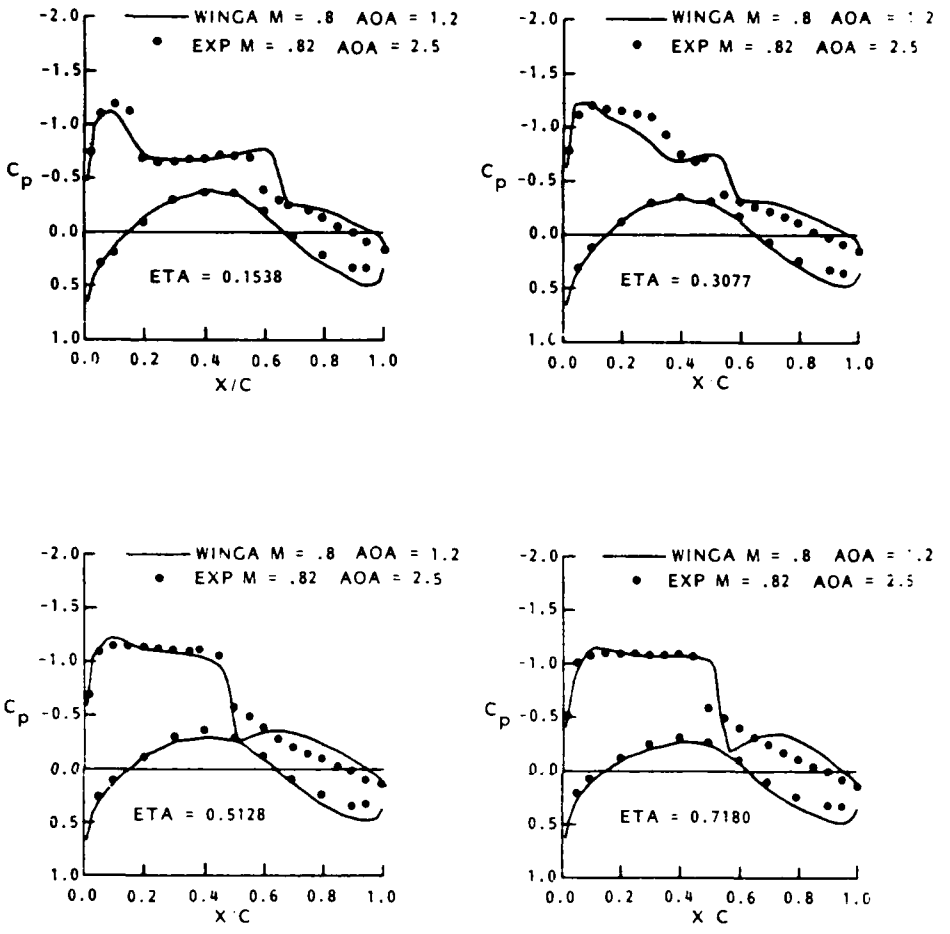

Figure 13. Correlation of WING A Analysis and Experimental Pressure Coefficients at $M_\infty = 0.80$, $\alpha = 1.2$

(Sheet 1 of 2)

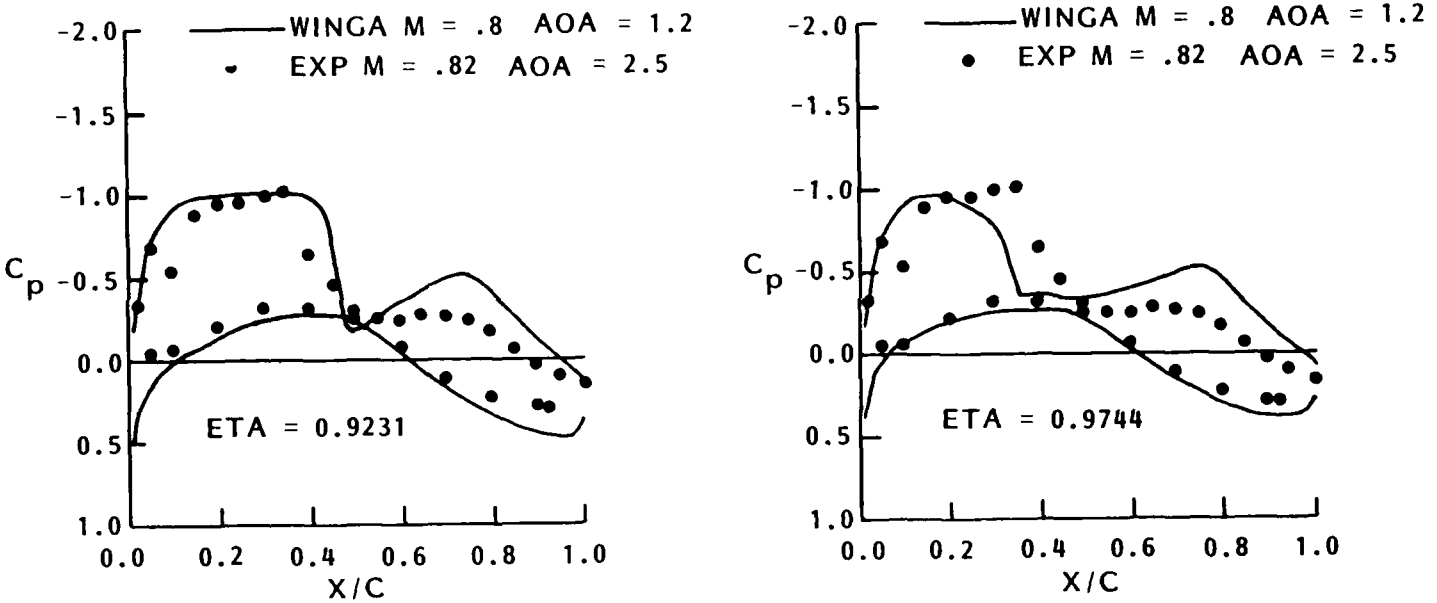

Figure 13. Correlation of WING A Analysis and Experimental Pressure Coefficients at $M\infty = 0.80$, $\alpha = 1.2$

(Sheet 2 of 2)

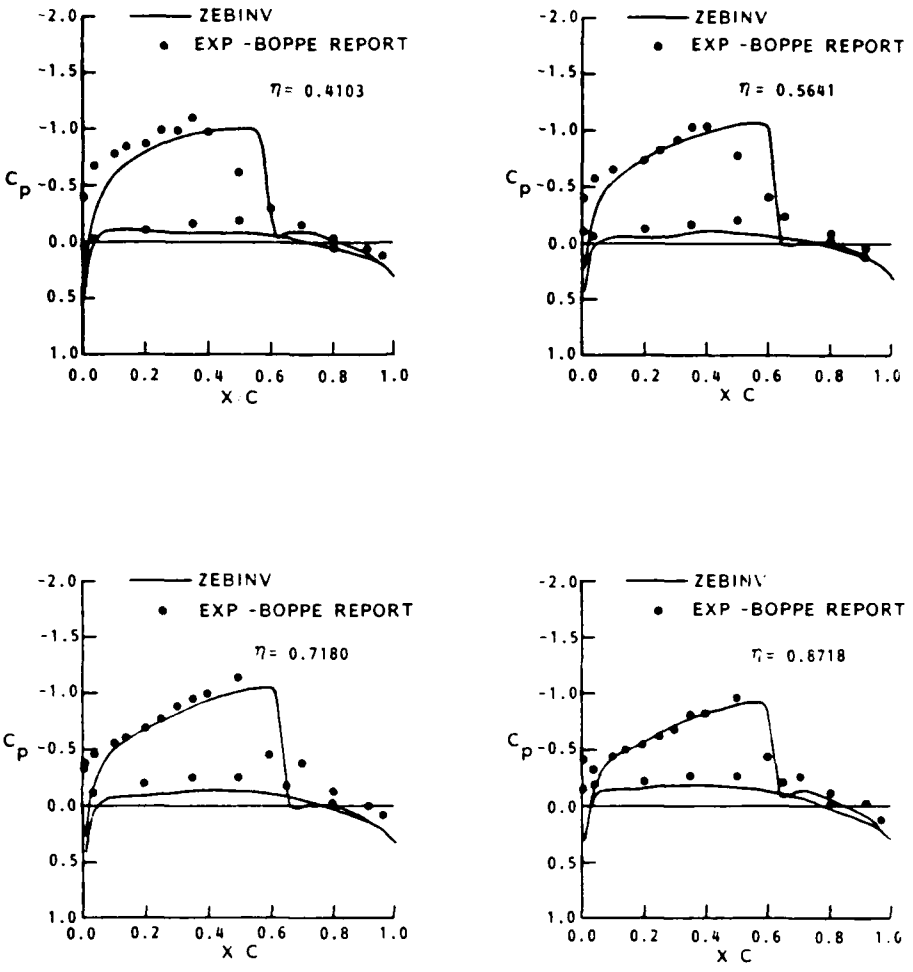

Figure 14. Correlation of F14A Analysis and Experimental Pressure Coefficient for $M\infty = 0.80$; $\alpha = 1.4$

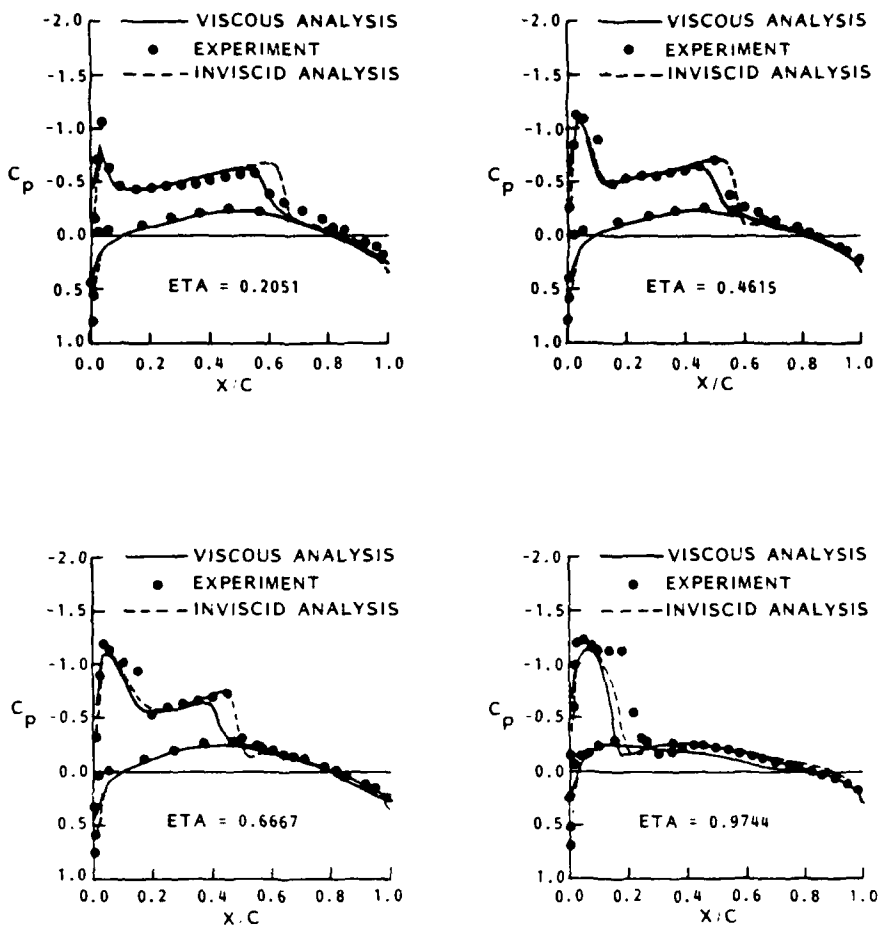

Figure 15. Correlation of Viscous ONERA M6 Wing Pressure Coefficient with Inviscid Analysis and Experiment at $M_\infty = 0.84$, $\alpha = 3.06$

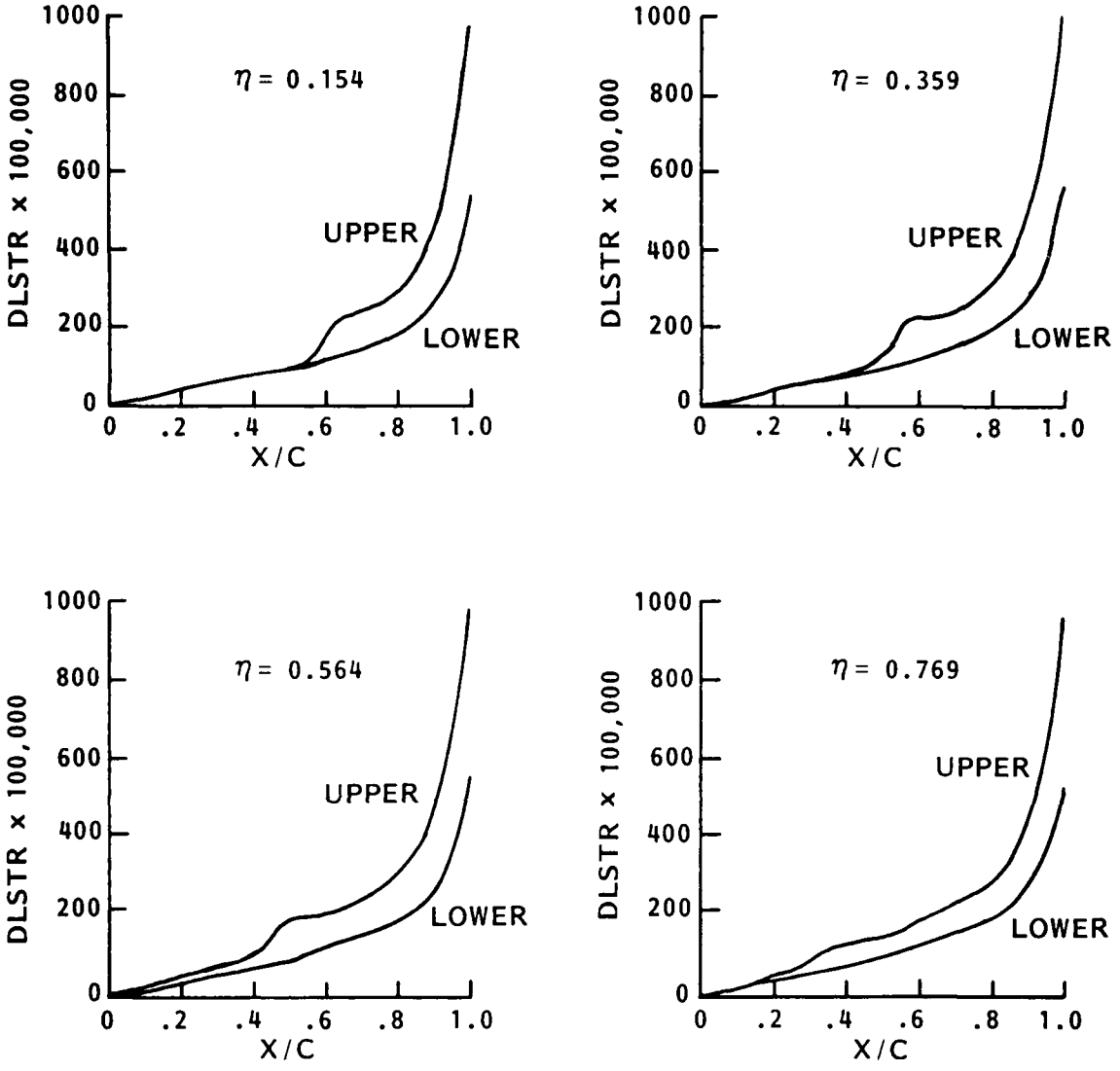

Figure 16. Typical Displacement Thickness Profiles at Various Span Stations on the ONERA M6 Wing

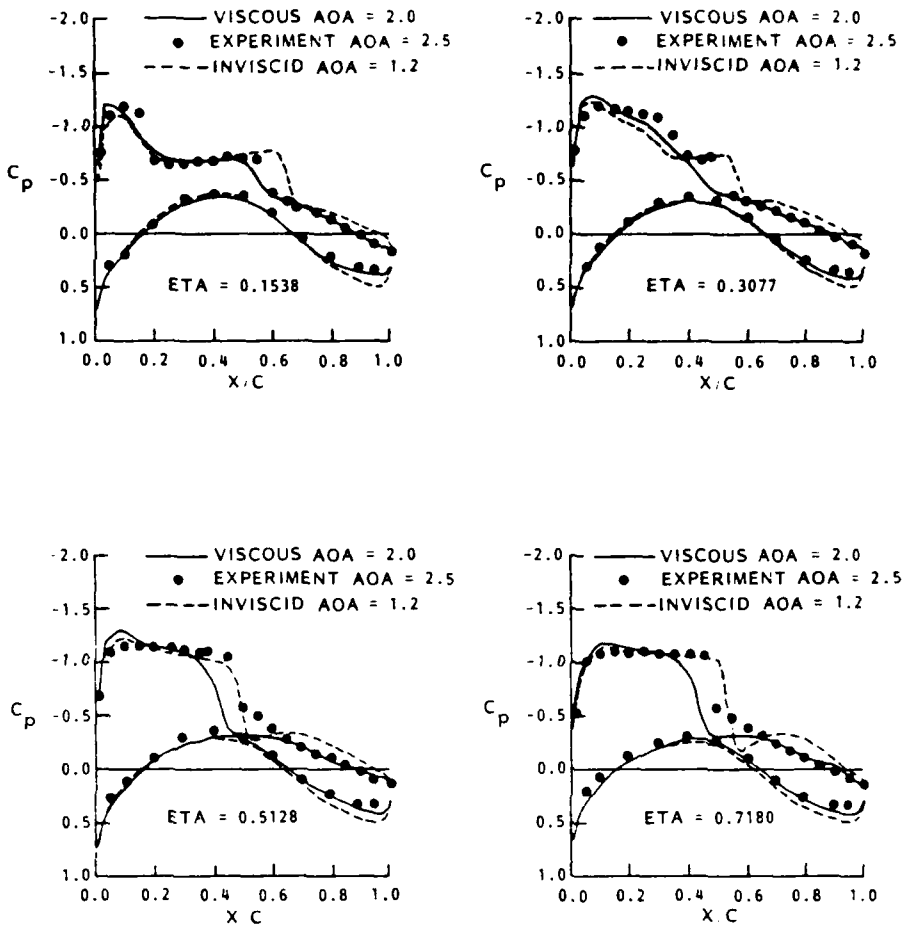

Figure 17. Correlation of Viscous WING A Pressure Coefficient with Inviscid Analysis and Experiment at $M_\infty = 0.80$, $\alpha = 1.2$

(Sheet 1 of 2)

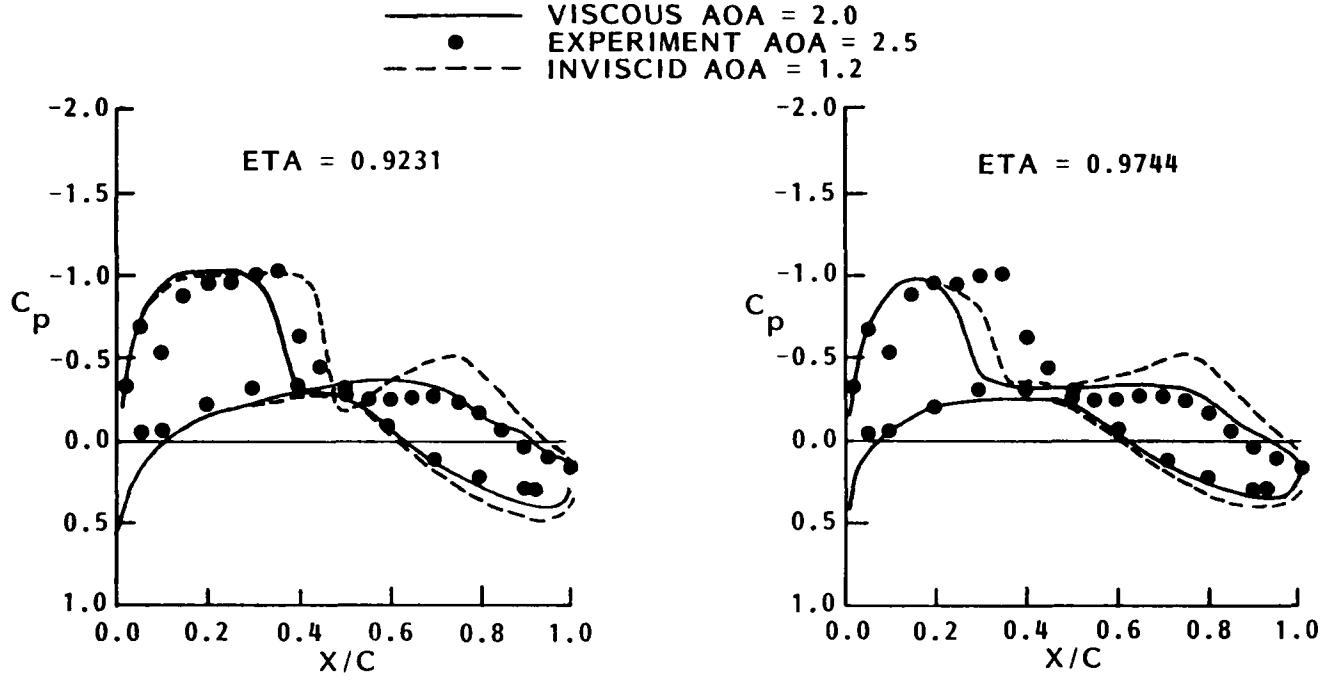

Figure 17. Correlation of Viscous WING A Pressure Coefficient with Inviscid Analysis and Experiment at $M\infty = 0.80$, $\alpha = 1.2$

(Sheet 2 of 2)

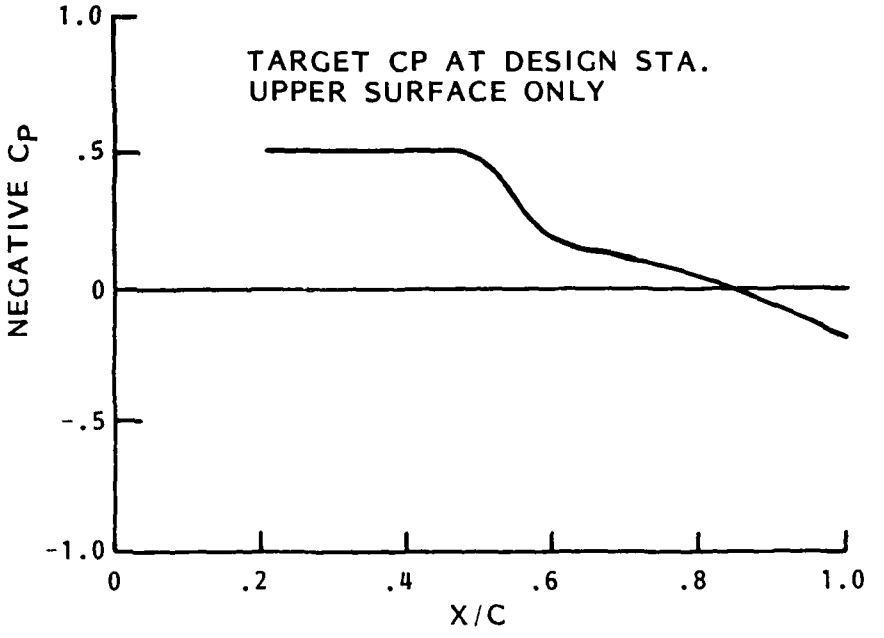

Figure 18. Upper Surface Target Pressure Distribution at the Design Station, η = 0.615

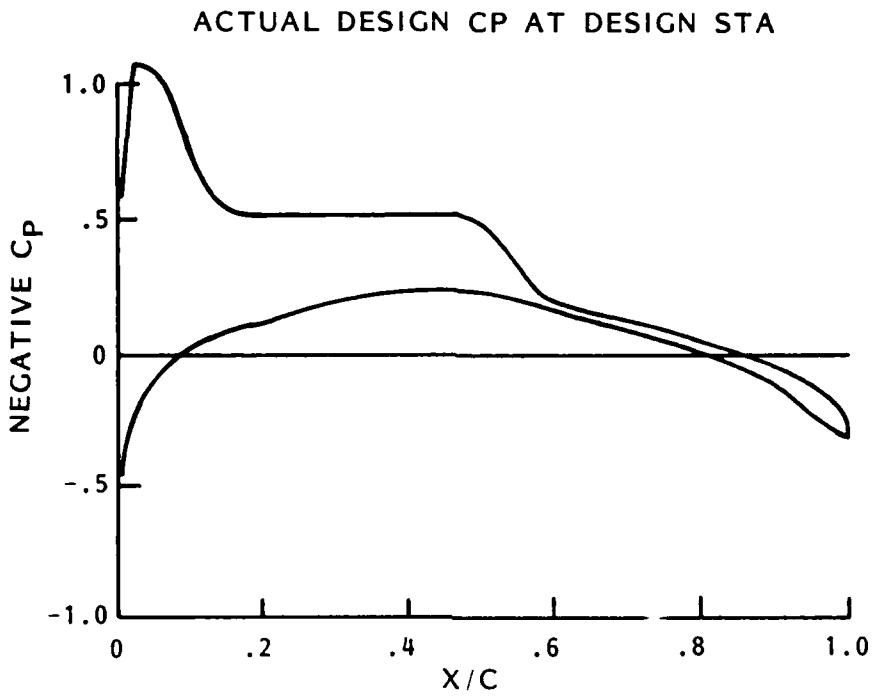

Figure 19. Actual Pressure Distribution at the Design Station

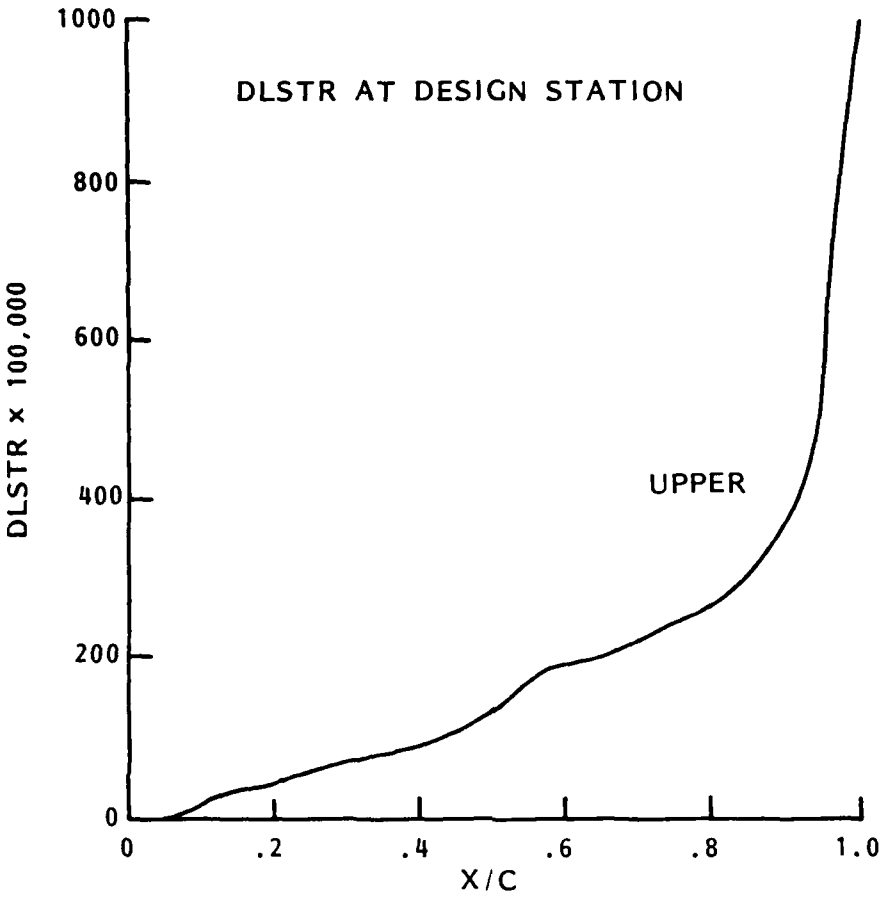

Figure 20. Upper Surface Displacement Surface Profile at the Design Station

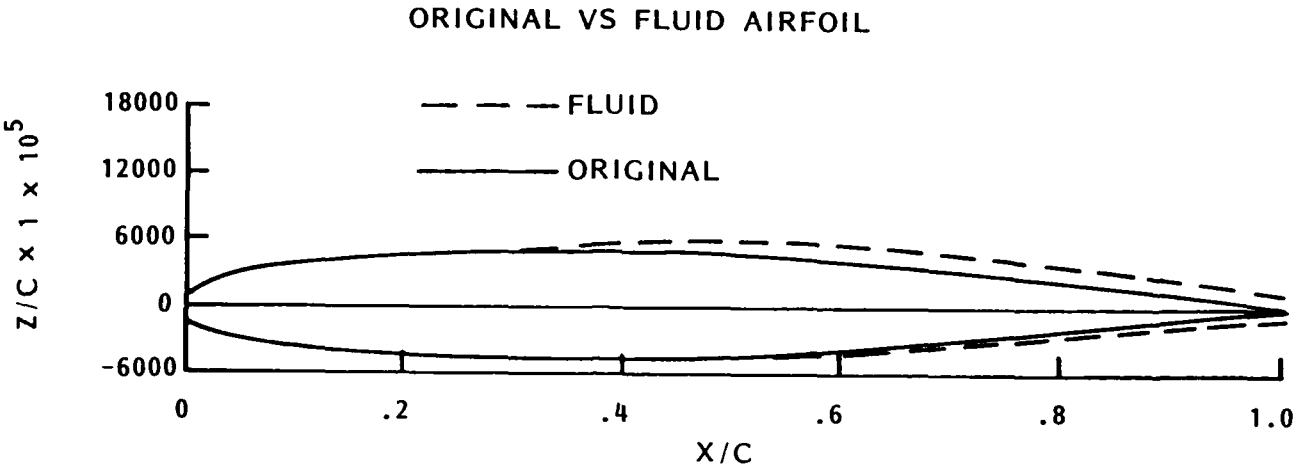

Figure 21. Comparison of the Original ONERA M6 Airfoil Section with the Fluid Airfoil Determined by the Design Method

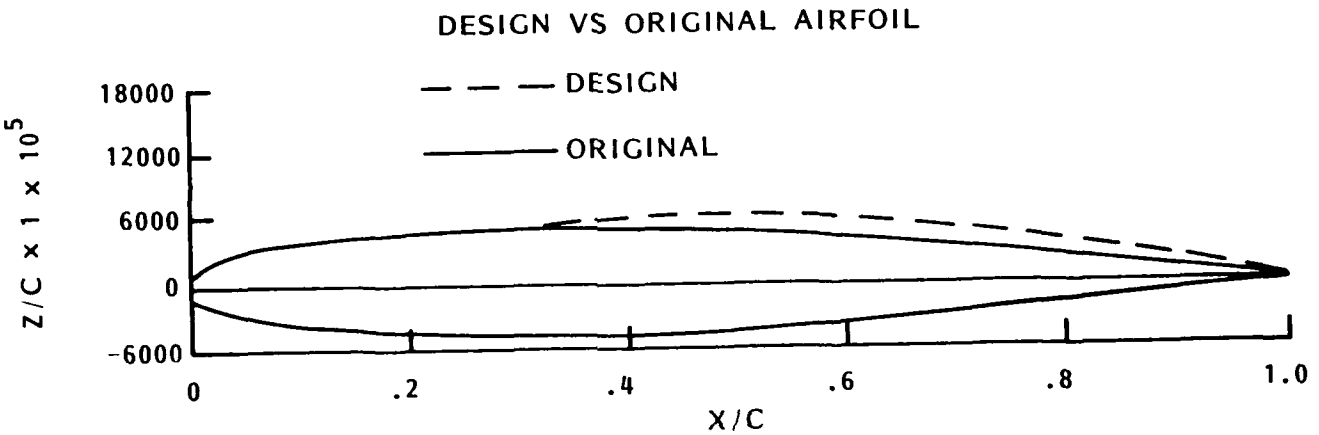

Figure 22. Comparison of the Original ONERA M6 Airfoil Section with the Section Designed by the Inverse Method

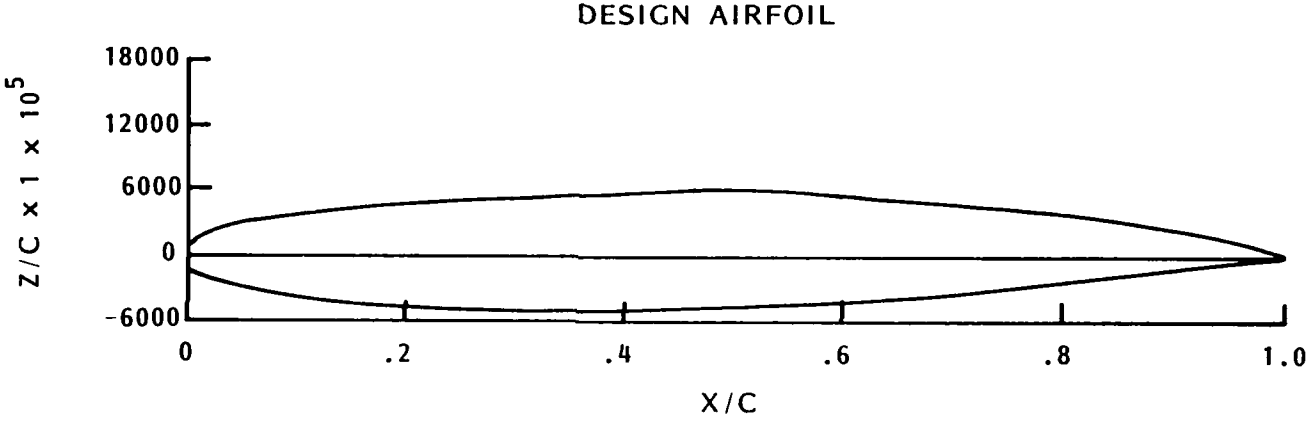

Figure 23. Airfoil Shape Determined by the Viscous Design Method at Span Station η = 0.615

APPENDIX A

WING PLANFORMS USED IN ANALYSIS AND DESIGN VERIFICATION

The wing planforms used in the verification of the analysis and design methods are shown in Figure A-1. These planforms were selected because both experimental and computational data was available for all the planforms at several test conditions. The wide variation in aspect ratio and taper ratio of the planforms provided realistic tests for both the analysis and design methods.

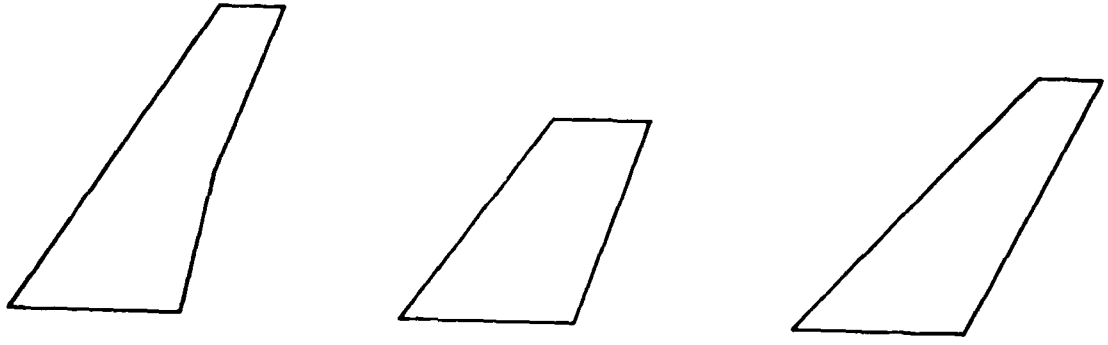

WING -	C5A	ONERA M6	RAE WING "A"
AR -	7.75	3.8	5.5
Λ_{LE} -	28°	30°	36.7°
λ -	0.37	0.56	0.38
θ_r -	0.0°	0.0°	0.0°
θ_t -	-3.5°	0.0°	0.0°

Figure A-1. Wing Planforms Used in Analysis and Design Verification Tests

(Sheet 1 of 2)

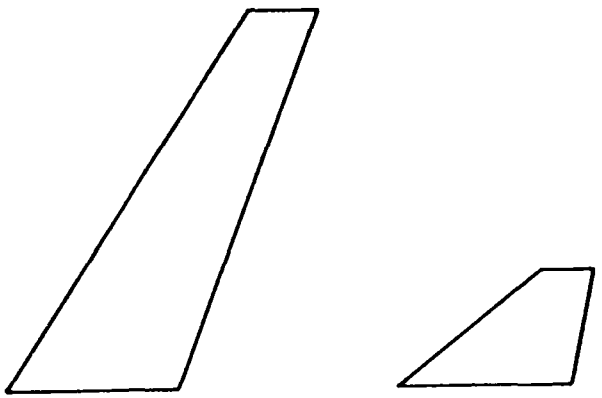

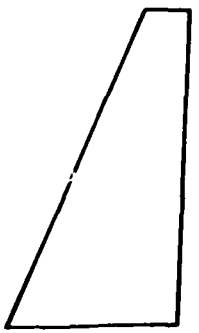

WING -	A	C	F14A (WING ALONE)
AR -	8.0	2.6	7.3
Λ_{LE} -	27°	45°	20°
λ -	0.4	0.3	0.26
θ_r -	2.57°	2.39	0.2°
θ_t -	-2.00°	-5.59	-3.40°

Figure A-1. Wing Planforms Used in Analysis and Design Verification Tests
(Sheet 2 of 2)

REFERENCES

1. Weed, R. A., Carlson L. A., and Anderson, W. K., "Combined Direct/Inverse Three-Dimensional Transonic Wing Design," DTNSRDC-ASED-CR-03-83, May 1983.

2. Carlson L. A., "Transonic Airfoil Design Using Cartesian Coordinates," NASA CR-2578, 1976.

3. Malone J. B., "A Subsonic Panel Method for Iterative Design of Complex Aircraft Configurations," Journal of Aircraft, Vol. 19, No. 10, 1982, pp. 820-825.

4. Narain J. P., "Incorporation of Body Effects into the FLO22NM Computer Code," Lockheed-Georgia Company Report No. LG81UG7274-304, December 1981.

5. Schlichting, H. and Truckenbrodt, E., Aerodynamics of the Airplane, McGraw-Hill, New York, 1979.

6. Treadgold, D. A., Jones, A. F., and Wilson, K. H., " Pressure Distribution Measured in the RAE 8ft X 6ft Transonic Wind Tunnel on RAE Wing °A° in Combination with an Axi-Symmetric Body at Mach Numbers of 0.4, 0.8, 0.9," AGARD-AR-138, May 1979.

7. Nash, J. F. and Tseng, R. R., "The Three Dimensional Turbulent Boundary Layer on an Infinite Yawed Wing," The Aeronautical Quarterly, November 1971, pp. 346-362.

8. Nash, J. F. and Macdonald, A. G. J., "The Calculation of Momentum Thickness in a Turbulent Boundary Layer at Mach Numbers up to Unity," Aero. Res. Council, C. P. No. 963, 1967.

9. Carlson, L. A., "TRANDES: A Fortran Program for Transonic Airfoil Analysis or Design," NASA Report CR-2821, June 1977.

10. Hinson, B. L. and Burdges, K. P., "Acquistion and Application of Transonic Wing and Far-Field Test Data for Three-Dimensional Computational Method Evaluation," AFOSR-TR-80-0421, March 1980.

11. Holst, T. L., Subramarian, N. R., and Thomas S. D., "The Efficient Solution of Transonic Wing Flow Fields," 2nd Symposium on Numerical and Physical Aspects of Aerodynamic Flows," January 1983.

12. Boppe, C. W. and Rosen B. S., "F14 Aircraft High Speed Flow Simulations," NASA CR-172559, April 1985.

DTIC

FILMED

4-86

END